

Notes on Koopman Operator Theory

Steven L. Brunton

Department of Mechanical Engineering, University of Washington, Seattle, WA 98195, United States

The classical geometric and statistical perspectives on dynamical systems are being complemented by a third *operator-theoretic* perspective, based on the evolution of measurements of the system. This so-called *Koopman* operator theory is poised to capitalize on the increasing availability of measurement data from complex systems. Moreover, Koopman theory provides a path to identify intrinsic coordinate systems where nonlinear dynamics appear linear. Obtaining linear representations of strongly nonlinear systems has the potential to revolutionize our ability to predict and control these systems. Sections of these notes are taken from the textbook *Data-Driven Science and Engineering: Machine Learning, Dynamical Systems, and Control* [12] by Brunton and Kutz.

1 Background on dynamical systems

Before summarizing recent developments in data-driven dynamical systems and Koopman theory, it is important to first provide a mathematical introduction to the notation and summarize key motivations and open challenges in dynamical systems.

1.1 Dynamical systems

Throughout these notes, we will consider dynamical systems of the form:

$$\frac{d}{dt}\mathbf{x}(t) = \mathbf{f}(\mathbf{x}(t), t; \boldsymbol{\beta}), \quad (1)$$

where \mathbf{x} is the state of the system and \mathbf{f} is a vector field that possibly depends on the state \mathbf{x} , time t , and a set of parameters $\boldsymbol{\beta}$.

We will often consider the simpler case of an autonomous system without time dependence or parameters:

$$\frac{d}{dt}\mathbf{x}(t) = \mathbf{f}(\mathbf{x}(t)). \quad (2)$$

Discrete-time systems

We will also consider the discrete-time dynamical system

$$\mathbf{x}_{k+1} = \mathbf{F}(\mathbf{x}_k). \quad (3)$$

Also known as a *map*, the discrete-time dynamics are more general than the continuous-time formulation in (2), encompassing discontinuous and hybrid systems as well.

Discrete-time dynamics may be induced from continuous-time dynamics, where \mathbf{x}_k is obtained by sampling the trajectory in (2) discretely in time, so that $\mathbf{x}_k = \mathbf{x}(k\Delta t)$. The discrete-time propagator $\mathbf{F}_{\Delta t}$ is now parameterized by the time step Δt . For an arbitrary time t , the *flow map* \mathbf{F}_t is defined as

$$\mathbf{F}_t(\mathbf{x}(t_0)) = \mathbf{x}(t_0) + \int_{t_0}^{t_0+t} \mathbf{f}(\mathbf{x}(\tau)) d\tau. \quad (4)$$

The discrete-time perspective is often more natural when considering experimental data and digital control.

Linear dynamics and spectral decomposition

Whenever possible, it is desirable to work with linear dynamics of the form

$$\frac{d}{dt}\mathbf{x} = \mathbf{A}\mathbf{x}. \quad (5)$$

Linear dynamical systems admit closed-form solutions, and there are a wealth of techniques for the analysis, prediction, numerical simulation, estimation, and control of such systems. The solution of (5) is given by

$$\mathbf{x}(t_0 + t) = e^{\mathbf{A}t}\mathbf{x}(t_0). \quad (6)$$

The dynamics are entirely characterized by the eigenvalues and eigenvectors of the matrix \mathbf{A} , given by the *spectral decomposition* (eigen-decomposition) of \mathbf{A} :

$$\mathbf{A}\mathbf{T} = \mathbf{T}\mathbf{\Lambda}. \quad (7)$$

When \mathbf{A} has n distinct eigenvalues, then $\mathbf{\Lambda}$ is a diagonal matrix containing the eigenvalues λ_j and \mathbf{T} is a matrix whose columns are the linearly independent eigenvectors ξ_j associated with eigenvalues λ_j . In this case, it is possible to write $\mathbf{A} = \mathbf{T}\mathbf{\Lambda}\mathbf{T}^{-1}$, and the solution in (6) becomes

$$\mathbf{x}(t_0 + t) = \mathbf{T}e^{\mathbf{\Lambda}t}\mathbf{T}^{-1}\mathbf{x}(t_0). \quad (8)$$

More generally, in the case of repeated eigenvalues, the matrix $\mathbf{\Lambda}$ will consist of Jordan blocks [57]. Note that the continuous-time system gives rise to a discrete-time dynamical system, with \mathbf{F}_t given by the solution map $\exp(\mathbf{A}t)$ in (6). In this case, the discrete-time eigenvalues are given by $e^{\lambda t}$.

The matrix \mathbf{T}^{-1} defines a transformation, $\mathbf{z} = \mathbf{T}^{-1}\mathbf{x}$, into intrinsic eigenvector coordinates, \mathbf{z} , where the dynamics become decoupled:

$$\frac{d}{dt}\mathbf{z} = \mathbf{\Lambda}\mathbf{z}. \quad (9)$$

In other words, each coordinate, z_j , only depends on itself, with simple dynamics

$$\frac{d}{dt}z_j = \lambda_j z_j. \quad (10)$$

Thus, it is highly desirable to work with linear systems, since it is possible to transform the system into eigenvector coordinates where the dynamics become decoupled. No such closed-form solution or simple linear change of coordinates exist in general for nonlinear systems, motivating many of the directions described in these notes.

1.2 Goals and challenges in modern dynamical systems

As we generally use dynamical systems to model real-world phenomena, there are a number of high-priority goals associated with the analysis of dynamical systems:

1. **Future state prediction.** In many cases, such as meteorology and climatology, we seek predictions of the future state of a system. Long-time predictions may still be challenging.
2. **Design and optimization.** We may seek to tune the parameters of a system for improved performance or stability, for example through the placement of fins on a rocket.
3. **Estimation and control.** It is often possible to actively control a dynamical system through feedback, using measurements of the system to inform actuation to modify the behavior. In this case, it is often necessary to estimate the full state of the system from limited measurements.
4. **Interpretability and physical understanding.** Perhaps a more fundamental goal of dynamical systems is to provide physical insight and interpretability into a system's behavior through analyzing trajectories and solutions to the governing equations of motion.

Real-world systems are generally nonlinear and exhibit multi-scale behavior in both space and time. It must also be assumed that there is uncertainty in the equations of motion, in the specification of parameters, and in the measurements of the system. Some systems are more sensitive to this uncertainty than others, and probabilistic approaches must be used. Increasingly, it is also the case that the basic equations of motion are not specified and they might be intractable to derive from first principles.

These notes will cover recent data-driven techniques to identify and analyze dynamical systems. The majority of these notes addresses two primary challenges of modern dynamical systems:

1. **Nonlinearity.** Nonlinearity remains a primary challenge in analyzing and controlling dynamical systems, giving rise to complex global dynamics. We saw above that linear systems may be completely characterized in terms of the spectral decomposition (i.e., eigenvalues and eigenvectors) of the matrix \mathbf{A} , leading to general procedures for prediction, estimation, and control. No such overarching framework exists for nonlinear systems, and developing this general framework is a mathematical grand challenge of the 21st century.

The leading perspective on nonlinear dynamical systems considers the geometry of subspaces of local linearizations around fixed points and periodic orbits, global heteroclinic and homoclinic orbits connecting these structures, and

more general attractors [25]. This geometric theory, originating with Poincaré, has transformed how we model complex systems, and its success can be largely attributed to theoretical results, such as the Hartman-Grobman theorem, which establish when and where it is possible to approximate a nonlinear system with linear dynamics. Thus, it is often possible to apply the wealth of linear analysis techniques in a small neighborhood of a fixed point or periodic orbit. Although the geometric perspective provides quantitative locally linear models, global analysis has remained largely qualitative and computational, limiting the theory of nonlinear prediction, estimation, and control away from fixed points and periodic orbits.

2. **Unknown dynamics.** Perhaps an even more central challenge arises from the lack of known governing equations for many modern systems of interest. Increasingly, researchers are tackling more complex and realistic systems, such as are found in neuroscience, epidemiology, and ecology. In these fields, there is a basic lack of known *physical laws* that provide first principles from which it is possible to derive equations of motion. Even in systems where we do know the governing equations, such as turbulence, protein folding, and combustion, we struggle to find patterns in these high-dimensional systems to uncover intrinsic coordinates and coarse-grained variables along which the dominant behavior evolves.

Traditionally, physical systems were analyzed by making ideal approximations and then deriving simple differential equation models via Newton's second law. Dramatic simplifications could often be made by exploiting symmetries and clever coordinate systems, as highlighted by the success of Lagrangian and Hamiltonian dynamics [1, 43]. With increasingly complex systems, the paradigm is shifting from this classical approach to data-driven methods to discover governing equations.

All models are approximations, and with increasing complexity, these approximations often become suspect. Determining what is the correct model is becoming more subjective, and there is a growing need for automated model discovery techniques that illuminate underlying physical mechanisms. There are also often latent variables that are relevant to the dynamics but may go unmeasured. Uncovering these hidden effects is a major challenge for data-driven methods.

Identifying unknown dynamics from data and learning intrinsic coordinates that enable the linear representation of nonlinear systems are two of the most pressing goals of modern dynamical systems. Overcoming the challenges of unknown dynamics and nonlinearity has the promise of transforming our understanding of complex systems, with tremendous potential benefit to nearly all fields of science and engineering.

To address the issue of nonlinearity, operator-theoretic approaches to dynamical systems are becoming increasingly used. As we will show, it is possible to represent nonlinear dynamical systems in terms of infinite-dimensional but linear operators, such as the Koopman operator from Sec. 2 that advances measurement functions, and the Perron-Frobenius operator that advances probability densities and ensembles through the dynamics.

2 Koopman operator theory

Koopman operator theory has recently emerged as an alternative perspective for dynamical systems in terms of the evolution of measurements $g(\mathbf{x})$. In 1931, Bernard O. Koopman demonstrated that it is possible to represent a nonlinear dynamical system in terms of an infinite-dimensional linear operator acting on a Hilbert space of measurement functions of the state of the system. This so-called *Koopman operator* is linear, and its spectral decomposition completely characterizes the behavior of a nonlinear system, analogous to (5). However, it is also infinite-dimensional, as there are infinitely many degrees of freedom required to describe the space of all possible measurement functions g of the state. This poses new challenges. Obtaining finite-dimensional, matrix approximations of the Koopman operator is the focus of intense research efforts and holds the promise of enabling globally linear representations of nonlinear dynamical systems. Expressing nonlinear dynamics in a linear framework is appealing because of the wealth of optimal estimation and control techniques available for linear systems and the ability to analytically predict the future state of the system. Obtaining a finite-dimensional approximation of the Koopman operator has been challenging in practice, as it involves identifying a subspace spanned by a subset of eigenfunctions of the Koopman operator.

2.1 Mathematical formulation of Koopman theory

The Koopman operator advances measurement functions of the state with the flow of the dynamics. We consider real-valued measurement functions $g : \mathbf{M} \rightarrow \mathbb{R}$, which are elements of an infinite-dimensional Hilbert space. The functions g are also commonly known as *observables*, although this may be confused with the unrelated *observability* from control theory. Typically, the Hilbert space is given by the Lebesgue square-integrable functions on \mathbf{M} ; other choices of a measure space are also valid.

The Koopman operator \mathcal{K}_t is an infinite-dimensional linear operator that acts on measurement functions g as:

$$\mathcal{K}_t g = g \circ \mathbf{F}_t \quad (11)$$

where \circ is the composition operator. For a discrete-time system with timestep Δt , this becomes:

$$\mathcal{K}_{\Delta t} g(\mathbf{x}_k) = g(\mathbf{F}_{\Delta t}(\mathbf{x}_k)) = g(\mathbf{x}_{k+1}). \quad (12)$$

In other words, the Koopman operator defines an infinite-dimensional linear dynamical system that advances the observation of the state $g_k = g(\mathbf{x}_k)$ to the next time step:

$$g(\mathbf{x}_{k+1}) = \mathcal{K}_{\Delta t} g(\mathbf{x}_k). \quad (13)$$

Note that this is true for *any* observable function g and for any state \mathbf{x}_k .

The Koopman operator is linear, a property which is inherited from the linearity of the addition operation in function spaces:

$$\mathcal{K}_t (\alpha_1 g_1(\mathbf{x}) + \alpha_2 g_2(\mathbf{x})) = \alpha_1 g_1(\mathbf{F}_t(\mathbf{x})) + \alpha_2 g_2(\mathbf{F}_t(\mathbf{x})) \quad (14a)$$

$$= \alpha_1 \mathcal{K}_t g_1(\mathbf{x}) + \alpha_2 \mathcal{K}_t g_2(\mathbf{x}). \quad (14b)$$

For sufficiently smooth dynamical systems, it is also possible to define the continuous-time analogue of the Koopman dynamical system in (13):

$$\frac{d}{dt}g = \mathcal{K}g. \quad (15)$$

The operator \mathcal{K} is the infinitesimal generator of the one-parameter family of transformations \mathcal{K}_t [2]. It is defined by its action on an observable function g :

$$\mathcal{K}g = \lim_{t \rightarrow 0} \frac{\mathcal{K}_t g - g}{t} = \lim_{t \rightarrow 0} \frac{g \circ \mathbf{F}_t - g}{t}. \quad (16)$$

The linear dynamical systems in (15) and (13) are analogous to the dynamical systems in (2) and (3), respectively. It is important to note that the original state \mathbf{x} may be the observable, and the infinite-dimensional operator \mathcal{K}_t will advance this function. However, the simple representation of the observable $g = \mathbf{x}$ in a chosen basis for Hilbert space may become arbitrarily complex once iterated through the dynamics. In other words, finding a representation for $\mathcal{K}\mathbf{x}$ may not be simple or straightforward.

Koopman eigenfunctions and intrinsic coordinates

The Koopman operator is linear, which is appealing, but is infinite dimensional, posing issues for representation and computation. Instead of capturing the evolution of all measurement functions in a Hilbert space, applied Koopman analysis attempts to identify key measurement functions that evolve linearly with the flow of the dynamics. Eigenfunctions of the Koopman operator provide just such a set of special measurements that behave linearly in time. In fact, a primary motivation to adopt the Koopman framework is the ability to simplify the dynamics through the eigen-decomposition of the operator.

A discrete-time Koopman eigenfunction $\varphi(\mathbf{x})$ corresponding to eigenvalue λ satisfies

$$\varphi(\mathbf{x}_{k+1}) = \mathcal{K}_{\Delta t} \varphi(\mathbf{x}_k) = \lambda \varphi(\mathbf{x}_k). \quad (17)$$

In continuous-time, a Koopman eigenfunction $\varphi(\mathbf{x})$ satisfies

$$\frac{d}{dt} \varphi(\mathbf{x}) = \mathcal{K} \varphi(\mathbf{x}) = \lambda \varphi(\mathbf{x}). \quad (18)$$

Obtaining Koopman eigenfunctions from data or from analytic expressions is a central applied challenge in modern dynamical systems. Discovering these eigenfunctions enables globally linear representations of strongly nonlinear systems.

Applying the chain rule to the time derivative of the Koopman eigenfunction $\varphi(\mathbf{x})$ yields

$$\frac{d}{dt} \varphi(\mathbf{x}) = \nabla \varphi(\mathbf{x}) \cdot \dot{\mathbf{x}} = \nabla \varphi(\mathbf{x}) \cdot \mathbf{f}(\mathbf{x}). \quad (19)$$

Combined with (18), this results in a partial differential equation (PDE) for the eigenfunction $\varphi(\mathbf{x})$:

$$\nabla \varphi(\mathbf{x}) \cdot \mathbf{f}(\mathbf{x}) = \lambda \varphi(\mathbf{x}). \quad (20)$$

With this nonlinear PDE, it is possible to approximate the eigenfunctions, either by solving for the Laurent series or with data via regression, both of which are explored below. This formulation assumes that the dynamics are both continuous and differentiable. The discrete-time dynamics in (3) are more general, although in many examples the continuous-time dynamics have a simpler representation than the discrete-time map for long times. For example, the simple Lorenz system has a simple continuous-time representation, yet is generally unrepresentable for even moderately long discrete-time updates.

The key takeaway from (17) and (18) is that the nonlinear dynamics become completely linear in eigenfunction coordinates, given by $\varphi(\mathbf{x})$. As a simple example, any conserved quantity of a dynamical system is a Koopman eigenfunction corresponding to eigenvalue $\lambda = 0$. This establishes a Koopman extension of the famous Noether's theorem [52], implying that any symmetry in the governing equations gives rise to a new Koopman eigenfunction with eigenvalue $\lambda = 0$. For example, the Hamiltonian energy function is a Koopman eigenfunction for a conservative system. In addition, the constant function $\varphi = 1$ is always a trivial eigenfunction corresponding to $\lambda = 0$ for every dynamical system.

Eigenvalue lattices. Interestingly, a set of Koopman eigenfunctions may be used to generate more eigenfunctions. In discrete time, we find that the product of two eigenfunctions $\varphi_1(\mathbf{x})$ and $\varphi_2(\mathbf{x})$ is also an eigenfunction

$$\mathcal{K}_t(\varphi_1(\mathbf{x})\varphi_2(\mathbf{x})) = \varphi_1(\mathbf{F}_t(\mathbf{x}))\varphi_2(\mathbf{F}_t(\mathbf{x})) \quad (21a)$$

$$= \lambda_1\lambda_2\varphi_1(\mathbf{x})\varphi_2(\mathbf{x}) \quad (21b)$$

corresponding to a new eigenvalue $\lambda_1\lambda_2$ given by the product of the two eigenvalues of $\varphi_1(\mathbf{x})$ and $\varphi_2(\mathbf{x})$.

In continuous time, the relationship becomes:

$$\mathcal{K}(\varphi_1\varphi_2) = \frac{d}{dt}(\varphi_1\varphi_2) \quad (22a)$$

$$= \dot{\varphi}_1\varphi_2 + \varphi_1\dot{\varphi}_2 \quad (22b)$$

$$= \lambda_1\varphi_1\varphi_2 + \lambda_2\varphi_1\varphi_2 \quad (22c)$$

$$= (\lambda_1 + \lambda_2)\varphi_1\varphi_2. \quad (22d)$$

Interestingly, this means that the set of Koopman eigenfunctions establishes a commutative monoid under point-wise multiplication; a monoid has the structure of a group, except that the elements need not have inverses. Thus, depending on the dynamical system, there may be a finite set of *generator* eigenfunction elements that may be used to construct all other eigenfunctions. The corresponding eigenvalues similarly form a lattice, based on the product $\lambda_1\lambda_2$ or sum $\lambda_1 + \lambda_2$, depending on whether the dynamics are in discrete time or continuous time. For example, given a linear system $\dot{x} = \lambda x$, then $\varphi(x) = x$ is an eigenfunction with eigenvalue λ . Moreover, $\varphi^\alpha = x^\alpha$ is also an eigenfunction with eigenvalue $\alpha\lambda$ for any α .

The continuous time and discrete time lattices are related in a simple way. If the continuous-time eigenvalues are given by λ , then the corresponding discrete-time

eigenvalues are given by $e^{\lambda t}$. Thus, the eigenvalue expressions in (21b) and (22d) are related as:

$$e^{\lambda_1 t} e^{\lambda_2 t} \varphi_1(\mathbf{x}) \varphi_2(\mathbf{x}) = e^{(\lambda_1 + \lambda_2)t} \varphi_1(\mathbf{x}) \varphi_2(\mathbf{x}). \quad (23)$$

As another simple demonstration of the relationship between continuous-time and discrete-time eigenvalues, consider the continuous-time definition in (16) applied to an eigenfunction:

$$\lim_{t \rightarrow 0} \frac{\mathcal{K}_t \varphi(\mathbf{x}) - \varphi(\mathbf{x})}{t} = \lim_{t \rightarrow 0} \frac{e^{\lambda t} \varphi(\mathbf{x}) - \varphi(\mathbf{x})}{t} = \lambda \varphi(\mathbf{x}). \quad (24)$$

2.2 Koopman mode decomposition and finite representations

Until now, we have considered scalar measurements of a system, and we uncovered special *eigen*-measurements that evolve linearly in time. However, we often take multiple measurements of a system. In extreme cases, we may measure the entire state of a high-dimensional spatial system, such as an evolving fluid flow. These measurements may then be arranged in a vector \mathbf{g} :

$$\mathbf{g}(\mathbf{x}) = \begin{bmatrix} g_1(\mathbf{x}) \\ g_2(\mathbf{x}) \\ \vdots \\ g_p(\mathbf{x}) \end{bmatrix}. \quad (25)$$

Each of the individual measurements may be expanded in terms of the eigenfunctions $\varphi_j(\mathbf{x})$, which provide a basis for Hilbert space:

$$g_i(\mathbf{x}) = \sum_{j=1}^{\infty} v_{ij} \varphi_j(\mathbf{x}). \quad (26)$$

Thus, the vector of observables, \mathbf{g} , may be similarly expanded:

$$\mathbf{g}(\mathbf{x}) = \begin{bmatrix} g_1(\mathbf{x}) \\ g_2(\mathbf{x}) \\ \vdots \\ g_p(\mathbf{x}) \end{bmatrix} = \sum_{j=1}^{\infty} \varphi_j(\mathbf{x}) \mathbf{v}_j, \quad (27)$$

where \mathbf{v}_j is the j -th *Koopman mode* associated with the eigenfunction φ_j .

For conservative dynamical systems, such as those governed by Hamiltonian dynamics, the Koopman operator is unitary. Thus, the Koopman eigenfunctions are orthonormal for conservative systems, and it is possible to compute the Koopman modes \mathbf{v}_j directly by projection:

$$\mathbf{v}_j = \begin{bmatrix} \langle \varphi_j, g_1 \rangle \\ \langle \varphi_j, g_2 \rangle \\ \vdots \\ \langle \varphi_j, g_p \rangle \end{bmatrix}, \quad (28)$$

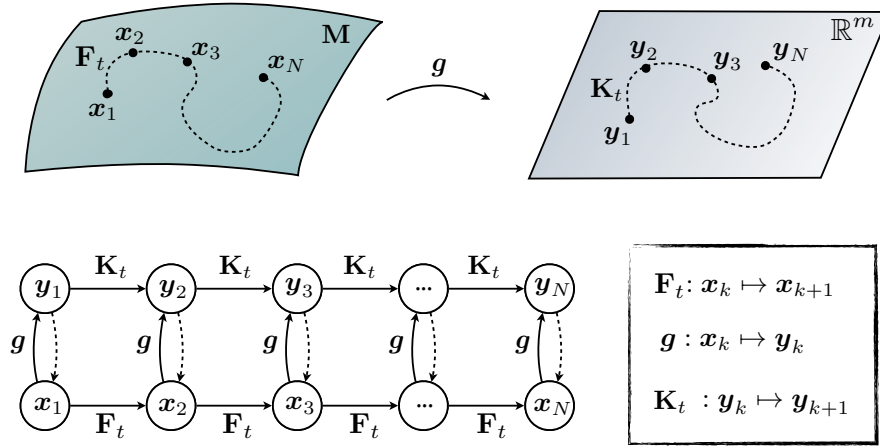


Figure 1: Schematic illustrating the Koopman operator for nonlinear dynamical systems. The dashed lines from $y_k \rightarrow x_k$ indicate that we would like to be able to recover the original state.

where $\langle \cdot, \cdot \rangle$ is the standard inner product of functions in Hilbert space. These modes have a physical interpretation in the case of direct spatial measurements of a system, $\mathbf{g}(\mathbf{x}) = \mathbf{x}$, in which case the modes are coherent *spatial* modes that behave linearly with the same temporal dynamics (i.e., oscillations, possibly with linear growth or decay).

Given the decomposition in (27), it is possible to represent the dynamics of the measurements \mathbf{g} as follows:

$$\mathbf{g}(\mathbf{x}_k) = \mathcal{K}_{\Delta t}^k \mathbf{g}(\mathbf{x}_0) = \mathcal{K}_{\Delta t}^k \sum_{j=0}^{\infty} \varphi_j(\mathbf{x}_0) \mathbf{v}_j \quad (29a)$$

$$= \sum_{j=0}^{\infty} \mathcal{K}_{\Delta t}^k \varphi_j(\mathbf{x}_0) \mathbf{v}_j \quad (29b)$$

$$= \sum_{j=0}^{\infty} \lambda_j^k \varphi_j(\mathbf{x}_0) \mathbf{v}_j. \quad (29c)$$

This sequence of triples, $\{(\lambda_j, \varphi_j, \mathbf{v}_j)\}_{j=0}^{\infty}$ is known as the *Koopman mode decomposition*, and was introduced by Mezic in 2005 [44]. The Koopman mode decomposition was later connected to data-driven regression via the dynamic mode decomposition [61].

Invariant eigenspaces and finite-dimensional models

Instead of capturing the evolution of all measurement functions in a Hilbert space, applied Koopman analysis approximates the evolution on an invariant subspace spanned by a finite set of measurement functions.

A *Koopman-invariant subspace* is defined as the span of a set of functions $\{g_1, g_2, \dots, g_p\}$ if all functions g in this subspace

$$g = \alpha_1 g_1 + \alpha_2 g_2 + \dots + \alpha_p g_p \quad (30)$$

remain in this subspace after being acted on by the Koopman operator \mathcal{K} :

$$\mathcal{K}g = \beta_1 g_1 + \beta_2 g_2 + \cdots + \beta_p g_p. \quad (31)$$

It is possible to obtain a finite-dimensional matrix representation of the Koopman operator by restricting it to an invariant subspace spanned by a finite number of functions $\{g_j\}_{j=0}^p$. The matrix representation \mathbf{K} acts on a vector space \mathbb{R}^p , with the coordinates given by the values of $g_j(\mathbf{x})$. This induces a finite-dimensional linear system, as in (13) and (15).

Any finite set of eigenfunctions of the Koopman operator will span an invariant subspace. Discovering these eigenfunction coordinates is, therefore, a central challenge, as they provide intrinsic coordinates along which the dynamics behave linearly. In practice, it is more likely that we will identify an *approximately* invariant subspace, given by a set of functions $\{g_j\}_{j=0}^p$, where each of the functions g_j is well approximated by a finite sum of eigenfunctions: $g_j \approx \sum_{k=0}^p \alpha_k \varphi_k$.

2.3 Examples of Koopman embeddings

Nonlinear system with single fixed point and a slow manifold

Here, we consider an example system with a single fixed point, given by:

$$\dot{x}_1 = \mu x_1 \quad (32a)$$

$$\dot{x}_2 = \lambda(x_2 - x_1^2). \quad (32b)$$

For $\lambda < \mu < 0$, the system exhibits a slow attracting manifold given by $x_2 = x_1^2$. It is possible to augment the state \mathbf{x} with the nonlinear measurement $g = x_1^2$, to define a three-dimensional Koopman invariant subspace. In these coordinates, the dynamics become linear:

$$\frac{d}{dt} \begin{bmatrix} y_1 \\ y_2 \\ y_3 \end{bmatrix} = \begin{bmatrix} \mu & 0 & 0 \\ 0 & \lambda & -\lambda \\ 0 & 0 & 2\mu \end{bmatrix} \begin{bmatrix} y_1 \\ y_2 \\ y_3 \end{bmatrix} \quad \text{for} \quad \begin{bmatrix} y_1 \\ y_2 \\ y_3 \end{bmatrix} = \begin{bmatrix} x_1 \\ x_2 \\ x_1^2 \end{bmatrix}. \quad (33a)$$

The full three-dimensional Koopman observable vector space is visualized in Fig. 2. Trajectories that start on the invariant manifold $y_3 = y_1^2$, visualized by the blue surface, are constrained to stay on this manifold. There is a *slow* subspace, spanned by the eigenvectors corresponding to the slow eigenvalues μ and 2μ ; this subspace is visualized by the green surface. Finally, there is the original asymptotically attracting manifold of the original system, $y_2 = y_1^2$, which is visualized as the red surface. The blue and red parabolic surfaces always intersect in a parabola that is inclined at a 45° angle in the y_2 - y_3 direction. The green surface approaches this 45° inclination as the ratio of fast to slow dynamics become increasingly large. In the full three-dimensional Koopman observable space, the dynamics produce a single stable node, with trajectories rapidly attracting onto the green subspace and then slowly approaching the fixed point.

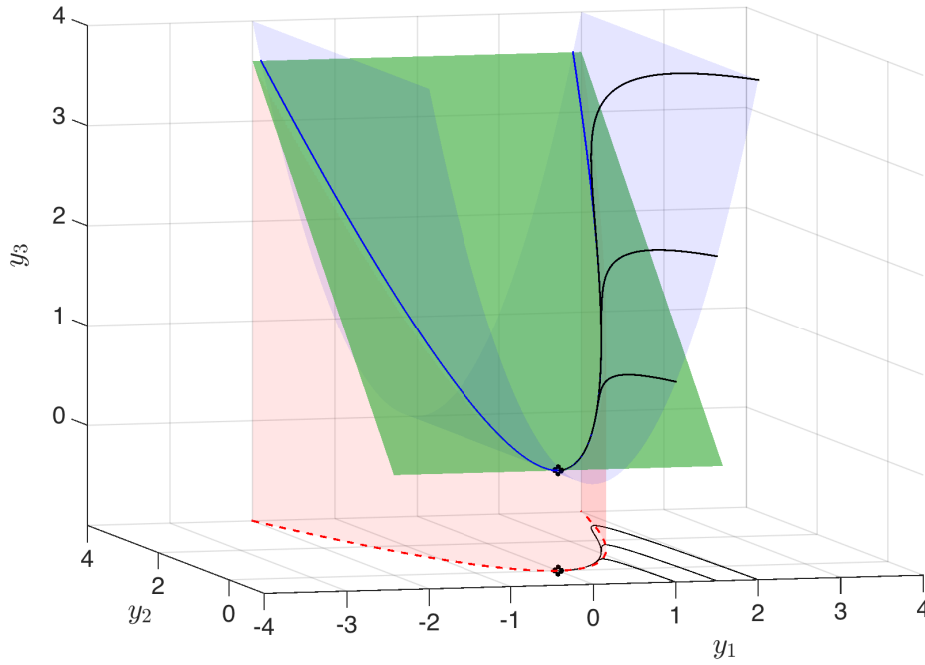


Figure 2: Visualization of three-dimensional linear Koopman system from (33a) along with projection of dynamics onto the x_1 - x_2 plane. The attracting slow manifold is shown in red, the constraint $y_3 = y_1^2$ is shown in blue, and the slow unstable subspace of (33a) is shown in green. Black trajectories of the linear Koopman system in \mathbf{y} project onto trajectories of the full nonlinear system in \mathbf{x} in the y_1 - y_2 plane. Here, $\mu = -0.05$ and $\lambda = 1$. *Reproduced from Brunton et al. [11].*

Intrinsic coordinates defined by eigenfunctions of the Koopman operator. The left eigenvectors of the Koopman operator yield Koopman eigenfunctions (i.e., eigenobservables). The Koopman eigenfunctions of (33a) corresponding to eigenvalues μ and λ are:

$$\varphi_\mu = x_1, \quad \text{and} \quad \varphi_\lambda = x_2 - bx_1^2 \quad \text{with} \quad b = \frac{\lambda}{\lambda - 2\mu}. \quad (34)$$

The constant b in φ_λ captures the fact that for a finite ratio λ/μ , the dynamics only shadow the asymptotically attracting slow manifold $x_2 = x_1^2$, but in fact follow neighboring parabolic trajectories. This is illustrated more clearly by the various surfaces in Fig. 2 for different ratios λ/μ .

In this way, a set of intrinsic coordinates may be determined from the observable functions defined by the left eigenvectors of the Koopman operator on an invariant subspace. Explicitly,

$$\varphi_\alpha(\mathbf{x}) = \xi_\alpha \mathbf{y}(\mathbf{x}), \quad \text{where} \quad \xi_\alpha \mathbf{K} = \alpha \xi_\alpha. \quad (35)$$

These eigen-observables define observable subspaces that remain invariant under the

Koopman operator, even after coordinate transformations. As such, they may be regarded as intrinsic coordinates [76] on the Koopman-invariant subspace.

Example of intractable representation

Consider the logistic map, given by:

$$x_{k+1} = \beta x_k(1 - x_k). \quad (36)$$

Let our observable subspace include x and x^2 :

$$\mathbf{y}_k = \begin{bmatrix} x \\ x^2 \end{bmatrix}_k \triangleq \begin{bmatrix} x_k \\ x_k^2 \end{bmatrix}. \quad (37)$$

Writing out the Koopman operator, the first row equation is simple:

$$\mathbf{y}_{k+1} = \begin{bmatrix} x \\ x^2 \end{bmatrix}_{k+1} = \begin{bmatrix} \beta & -\beta \\ ? & ? \end{bmatrix} \begin{bmatrix} x \\ x^2 \end{bmatrix}_k, \quad (38)$$

but the second row is not obvious. To find this expression, expand x_{k+1}^2 :

$$x_{k+1}^2 = (\beta x_k(1 - x_k))^2 = \beta^2 (x_k^2 - 2x_k^3 + x_k^4). \quad (39)$$

Thus, cubic and quartic polynomial terms are required to advance x^2 . Similarly, these terms need polynomials up to sixth and eighth order, respectively, and so on, ad infinitum:

$$\begin{bmatrix} x \\ x^2 \\ x^3 \\ x^4 \\ x^5 \\ \vdots \end{bmatrix}_{k+1} = \begin{bmatrix} \beta & -\beta & 0 & 0 & 0 & 0 & 0 & 0 & 0 & 0 & \cdots \\ 0 & \beta^2 & -2\beta^2 & \beta^2 & 0 & 0 & 0 & 0 & 0 & 0 & \cdots \\ 0 & 0 & \beta^3 & -3\beta^3 & 3\beta^3 & \beta^3 & 0 & 0 & 0 & 0 & \cdots \\ 0 & 0 & 0 & \beta^4 & -4\beta^4 & 6\beta^4 & -4\beta^4 & \beta^4 & 0 & 0 & \cdots \\ 0 & 0 & 0 & 0 & \beta^5 & -5\beta^5 & 10\beta^5 & -10\beta^5 & 5\beta^5 & -\beta^5 & \cdots \\ \vdots & \ddots \end{bmatrix} \begin{bmatrix} x \\ x^2 \\ x^3 \\ x^4 \\ x^5 \\ \vdots \end{bmatrix}_k.$$

It is interesting to note that the rows of this equation are related to the rows of Pascal's triangle, with the n -th row scaled by r^n , and with the omission of the first row:

$$[x^0]_{k+1} = [0] [x^0]_k. \quad (40)$$

The above representation of the Koopman operator in a polynomial basis is somewhat troubling. Not only is there no closure, but the determinant of any finite-rank truncation is very large for $\beta > 1$. This illustrates a pitfall associated with naive representation of the infinite dimensional Koopman operator for a simple chaotic system. Truncating the system, or performing a least squares fit on an augmented observable vector (i.e., DMD on a nonlinear measurement; see Sec. 3) yields poor results, with the truncated system only agreeing with the true dynamics for a small handful of iterations, as the complexity of the representation grows quickly:

$$\begin{array}{c} 1 \\ x \\ x^2 \\ x^3 \\ x^4 \\ x^5 \\ x^6 \\ x^7 \\ x^8 \\ \vdots \end{array} \begin{bmatrix} 0 \\ 1 \\ 0 \\ 0 \\ 0 \\ 0 \\ 0 \\ 0 \\ 0 \\ \vdots \end{bmatrix} \xrightarrow{\mathcal{K}} \begin{bmatrix} 0 \\ \beta \\ -\beta \\ 0 \\ 0 \\ 0 \\ 0 \\ 0 \\ 0 \\ \vdots \end{bmatrix} \xrightarrow{\mathcal{K}} \begin{bmatrix} 0 \\ \beta^2 \\ -\beta^2 - \beta^3 \\ 2\beta^3 \\ -\beta^3 \\ 0 \\ 0 \\ 0 \\ 0 \\ \vdots \end{bmatrix} \xrightarrow{\mathcal{K}} \begin{bmatrix} 0 \\ \beta^3 \\ -\beta^3 - \beta^4 - \beta^5 \\ 2\beta^4 + 2\beta^5 + 2\beta^6 \\ -\beta^4 - \beta^5 - 6\beta^6 - \beta^7 \\ 6\beta^6 + 4\beta^7 \\ -2\beta^6 - 6\beta^7 \\ 4\beta^7 \\ -\beta^7 \\ \vdots \end{bmatrix}. \quad (41)$$

2.4 Analytic series expansions for eigenfunctions

Given the dynamics in (1), it is possible to solve the PDE in (20) using standard techniques, such as recursively solving for the terms in a Taylor or Laurent series. A number of simple examples are explored below.

Linear dynamics.

Consider the simple linear dynamics

$$\frac{d}{dt}x = x. \quad (42)$$

Assuming a Taylor series expansion for $\varphi(x)$:

$$\varphi(x) = c_0 + c_1x + c_2x^2 + c_3x^3 + \dots$$

then the gradient and directional derivatives are given by:

$$\begin{aligned} \nabla\varphi &= c_1 + 2c_2x + 3c_3x^2 + 4c_4x^3 + \dots \\ \nabla\varphi \cdot f &= c_1x + 2c_2x^2 + 3c_3x^3 + 4c_4x^4 + \dots \end{aligned}$$

Solving for terms in the Koopman eigenfunction PDE (20), we see that $c_0 = 0$ must hold. For any positive integer λ in (20), only one of the coefficients may be nonzero. Specifically, for $\lambda = k \in \mathbb{Z}^+$, then $\varphi(x) = cx^k$ is an eigenfunction for any constant c . For instance, if $\lambda = 1$, then $\varphi(x) = x$.

Quadratic nonlinear dynamics

Consider a nonlinear dynamical system

$$\frac{d}{dt}x = x^2. \quad (43)$$

There is no Taylor series that satisfies (20), except the trivial solution $\varphi = 0$ for $\lambda = 0$. Instead, we assume a Laurent series:

$$\begin{aligned} \varphi(x) = & \cdots + c_{-3}x^{-3} + c_{-2}x^{-2} + c_{-1}x^{-1} + c_0 \\ & + c_1x + c_2x^2 + c_3x^3 + \cdots . \end{aligned}$$

The gradient and directional derivatives are given by:

$$\begin{aligned} \nabla\varphi = & \cdots - 3c_{-3}x^{-4} - 2c_{-2}x^{-3} - c_{-1}x^{-2} + c_1 + 2c_2x \\ & + 3c_3x^2 + 4c_4x^3 + \cdots \\ \nabla\varphi \cdot f = & \cdots - 3c_{-3}x^{-2} - 2c_{-2}x^{-1} - c_{-1} + c_1x^2 + 2c_2x^3 \\ & + 3c_3x^4 + 4c_4x^5 + \cdots . \end{aligned}$$

Solving for the coefficients of the Laurent series that satisfy (20), we find that all coefficients with positive index are zero, i.e. $c_k = 0$ for all $k \geq 1$. However, the nonpositive index coefficients are given by the recursion $\lambda c_{k+1} = kc_k$, for negative $k \leq -1$. Thus, the Laurent series is

$$\varphi(x) = c_0 \left(1 - \lambda x^{-1} + \frac{\lambda^2}{2} x^{-2} - \frac{\lambda^3}{3!} x^{-3} + \cdots \right) = c_0 e^{-\lambda/x}.$$

This holds for all values of $\lambda \in \mathbb{C}$. There are also other Koopman eigenfunctions that can be identified from the Laurent series.

Polynomial nonlinear dynamics

For a more general nonlinear dynamical system

$$\frac{d}{dt} = ax^n, \tag{44}$$

$\varphi(x) = e^{\frac{\lambda}{(1-n)a} x^{1-n}}$ is an eigenfunction for all $\lambda \in \mathbb{C}$.

As mentioned above, it is also possible to generate new eigenfunctions by taking powers of these primitive eigenfunctions; the resulting eigenvalues generate a *lattice* in the complex plane.

2.5 History and recent developments

The original analysis of Koopman in 1931 was introduced to describe the evolution of measurements of Hamiltonian systems [30], and this theory was generalized by Koopman and von Neumann to systems with continuous eigenvalue spectrum in 1932 [31]. In the case of Hamiltonian flows, the Koopman operator \mathcal{K}_t is unitary, and forms a one-parameter family of unitary transformations in Hilbert space. Unitary operators should be familiar by now, as the discrete Fourier transform (DFT) and the singular value decomposition (SVD) both provide unitary coordinate transformations. Unitarity implies that the inner product of any two observable functions remains unchanged through action of the Koopman operator, which is intuitively related to the

phase-space volume preserving property of Hamiltonian systems. In the original paper [30], Koopman drew connections between the Koopman eigenvalue spectrum and conserved quantities, integrability, and ergodicity. Interestingly, Koopman's 1931 paper was central in the celebrated proofs of the ergodic theorem by Birkhoff and von Neumann [7, 50, 8, 49].

Koopman analysis has recently gained renewed interest with the pioneering work of Mezic and collaborators [47, 44, 14, 16, 15, 45, 36]. The Koopman operator is also known as the composition operator, which is formally the pull-back operator on the space of scalar observable functions [2], and it is the dual, or left-adjoint, of the Perron-Frobenius operator, or transfer operator, which is the push-forward operator on the space of probability density functions. When a polynomial basis is chosen to represent the Koopman operator, then it is closely related to Carleman linearization [18, 19, 20], which has been used extensively in nonlinear control [66, 34, 6, 71]. Koopman analysis is also connected to the resolvent operator theory from fluid dynamics [65].

Recently, it has been shown that the operator theoretic framework complements the traditional geometric and probabilistic perspectives. For example, level sets of Koopman eigenfunctions form invariant partitions of the state-space of a dynamical system [15]; in particular, eigenfunctions of the Koopman operator may be used to analyze the ergodic partition [48, 14]. Koopman analysis has also been recently shown to generalize the Hartman-Grobman theorem to the entire basin of attraction of a stable or unstable equilibrium point or periodic orbit [36].

At the time of this writing, representing Koopman eigenfunctions for general dynamical systems remains a central unsolved challenge. Significant research efforts are focused on developing data-driven techniques to identify Koopman eigenfunctions and use these for control, which will be discussed in the following sections and chapters. Recently, new work has emerged that attempts to leverage the power of deep learning to discover and represent eigenfunctions from data [75, 42, 72, 78, 55, 38].

3 Data-driven Koopman analysis

Obtaining linear representations for strongly nonlinear systems has the potential to revolutionize our ability to predict and control these systems. The linearization of dynamics near fixed points or periodic orbits has long been employed for *local* linear representation of the dynamics [25]. The Koopman operator is appealing because it provides a *global* linear representation, valid far away from fixed points and periodic orbits. However, previous attempts to obtain finite-dimensional approximations of the Koopman operator have had limited success. Dynamic mode decomposition [63, 61, 35] seeks to approximate the Koopman operator with a best-fit linear model advancing spatial measurements from one time to the next, although these linear measurements are not rich enough for many nonlinear systems. Augmenting DMD with nonlinear measurements may enrich the model, but there is no guarantee that the resulting models will be closed under the Koopman operator [11]. Here, we describe several approaches for identifying Koopman embeddings and eigenfunctions from data. These methods include the extended dynamic mode decomposition [76], extensions based on SINDy [28], and the use of delay coordinates [10].

3.1 Dynamic mode decomposition (DMD)

Dynamic mode decomposition was developed by Schmid [64, 63] in the fluid dynamics community to identify spatio-temporal coherent structures from high-dimensional data. DMD is based on proper orthogonal decomposition (POD), which utilizes the computationally efficient singular value decomposition (SVD), so that it scales well to provide effective dimensionality reduction in high-dimensional systems. In contrast to SVD/POD, which results in a hierarchy of modes based entirely on spatial correlation and energy content, while largely ignoring temporal information, DMD provides a modal decomposition where each mode consists of spatially correlated structures that have the same linear behavior in time (e.g., oscillations at a given frequency with growth or decay). Thus, DMD not only provides dimensionality reduction in terms of a reduced set of modes, but also provides a model for how these modes evolve in time.

Soon after the development of the original DMD algorithm [64, 63], Rowley, Mezić, and collaborators established an important connection between DMD and Koopman theory [61] (see Sec. 2). DMD may be formulated as an algorithm to identify the best-fit linear dynamical system that advances high-dimensional measurements forward in time [74]. In this way, DMD approximates the Koopman operator restricted to the set of direct measurements of the state of a high-dimensional system. This connection between the computationally straightforward and linear DMD framework and nonlinear dynamical systems has generated considerable interest in these methods [35].

Within a short amount of time, DMD has become a workhorse algorithm for the data-driven characterization of high-dimensional systems. DMD is equally valid for experimental and numerical data, as it is not based on knowledge of the governing equations, but is instead based purely on measurement data. The DMD algorithm may also be seen as connecting the favorable aspects of the SVD for spatial dimensionality reduction and the FFT for temporal frequency identification [21, 35]. Thus, each DMD

mode is associated with a particular *eigenvalue* $\lambda = a + ib$, with a particular frequency of oscillation b and growth or decay rate a .

There are many variants of DMD and it is connected to existing techniques from system identification and modal extraction. DMD has become especially popular in recent years in large part due to its simple numerical implementation and strong connections to nonlinear dynamical systems via Koopman spectral theory. Finally, DMD is an extremely flexible platform, both mathematically and numerically, facilitating innovations related to compressed sensing, control theory, and multi-resolution techniques. These connections and extensions will be discussed at the end of this section.

3.2 The DMD algorithm

Several algorithms have been proposed for DMD, although here we present the *exact* DMD framework developed by Tu et al. [74]. Whereas earlier formulations required uniform sampling of the dynamics in time, the approach presented here works with irregularly sampled data and with concatenated data from several different experiments or numerical simulations. Moreover, the exact formulation of Tu et al. provides a precise mathematical definition of DMD that allows for rigorous theoretical results. Finally, exact DMD is based on the efficient and numerically well-conditioned singular value decomposition, as is the original formulation by Schmid [63].

DMD is inherently data-driven, and the first step is to collect a number of pairs of snapshots of the state of a system as it evolves in time. These snapshot pairs may be denoted by $\{\mathbf{x}(t_k), \mathbf{x}(t'_k)\}_{k=1}^m$, where $t'_k = t_k + \Delta t$, and the timestep Δt is sufficiently small to resolve the highest frequencies in the dynamics. As before, a snapshot may be the state of a system, such as a three-dimensional fluid velocity field sampled at a number of discretized locations, that is reshaped into a high-dimensional column vector. These snapshots are then arranged into two data matrices, \mathbf{X} and \mathbf{X}' :

$$\mathbf{X} = \begin{bmatrix} | & | & \cdots & | \\ \mathbf{x}(t_1) & \mathbf{x}(t_2) & \cdots & \mathbf{x}(t_m) \\ | & | & \cdots & | \end{bmatrix} \quad (45a)$$

$$\mathbf{X}' = \begin{bmatrix} | & | & \cdots & | \\ \mathbf{x}(t'_1) & \mathbf{x}(t'_2) & \cdots & \mathbf{x}(t'_m) \\ | & | & \cdots & | \end{bmatrix}. \quad (45b)$$

The original formulations of Schmid [63] and Rowley et al. [61] assumed uniform sampling in time, so that $t_k = k\Delta t$ and $t'_k = t_k + \Delta t = t_{k+1}$. If we assume uniform sampling in time, we will adopt the notation $\mathbf{x}_k = \mathbf{x}(k\Delta t)$.

The DMD algorithm seeks the leading spectral decomposition (i.e., eigenvalues and eigenvectors) of the best-fit linear operator \mathbf{A} that relates the two snapshot matrices in time:

$$\mathbf{X}' \approx \mathbf{A}\mathbf{X}. \quad (46)$$

The best fit operator \mathbf{A} then establishes a linear dynamical system that best advances snapshot measurements forward in time. If we assume uniform sampling in time, this

becomes:

$$\mathbf{x}_{k+1} \approx \mathbf{A}\mathbf{x}_k. \quad (47)$$

Mathematically, the best-fit operator \mathbf{A} is defined as

$$\mathbf{A} = \underset{\mathbf{A}}{\operatorname{argmin}} \|\mathbf{X}' - \mathbf{A}\mathbf{X}\|_F = \mathbf{X}'\mathbf{X}^\dagger \quad (48)$$

where $\|\cdot\|_F$ is the Frobenius norm and † denotes the pseudo-inverse. The optimized DMD algorithm generalizes the optimization framework of exact DMD to perform a regression to exponential time dynamics, thus providing an improved computation of the DMD modes and their eigenvalues [4].

It is worth noting at this point that the matrix \mathbf{A} in (47) closely resembles the Koopman operator in (13), if we choose direct linear measurements of the state, so that $\mathbf{g}(\mathbf{x}) = \mathbf{x}$. This connection was originally established by Rowley, Mezic and collaborators [61], and has sparked considerable interest in both DMD and Koopman theory. These connections will be explored in more depth below.

For a high-dimensional state vector $\mathbf{x} \in \mathbb{R}^n$, the matrix \mathbf{A} has n^2 elements, and representing this operator, let alone computing its spectral decomposition, may be intractable. Instead, the DMD algorithm leverages dimensionality reduction to compute the dominant eigenvalues and eigenvectors of \mathbf{A} without requiring any explicit computations using \mathbf{A} directly. In particular, the pseudo-inverse \mathbf{X}^\dagger in (48) is computed via the singular value decomposition of the matrix \mathbf{X} . Since this matrix typically has far fewer columns than rows, i.e. $m \ll n$, there are at most m non-zero singular values and corresponding singular vectors, and hence the matrix \mathbf{A} will have at most rank m . Instead of computing \mathbf{A} directly, we compute the projection of \mathbf{A} onto these leading singular vectors, resulting in a small matrix $\tilde{\mathbf{A}}$ of size at most $m \times m$. A major contribution of Schmid [63] was a procedure to approximate the high-dimensional DMD modes (eigenvectors of \mathbf{A}) from the reduced matrix $\tilde{\mathbf{A}}$ and the data matrix \mathbf{X} without ever resorting to computations on the full \mathbf{A} . Tu et al. [74] later proved that these approximate modes are in fact exact eigenvectors of the full \mathbf{A} matrix under certain conditions. Thus, the exact DMD algorithm of Tu et al. [74] is given by the following steps:

Step 1. Compute the singular value decomposition of \mathbf{X} :

$$\mathbf{X} \approx \tilde{\mathbf{U}}\tilde{\Sigma}\tilde{\mathbf{V}}^*, \quad (49)$$

where $\tilde{\mathbf{U}} \in \mathbb{C}^{n \times r}$, $\tilde{\Sigma} \in \mathbb{C}^{r \times r}$, and $\tilde{\mathbf{V}} \in \mathbb{C}^{m \times r}$ and $r \leq m$ denotes either the exact or approximate rank of the data matrix \mathbf{X} . In practice, choosing the approximate rank r is one of the most important and subjective steps in DMD, and in dimensionality reduction in general. We advocate the principled hard-thresholding algorithm of Gavish and Donoho [24] to determine r from noisy data. The columns of the matrix $\tilde{\mathbf{U}}$ are also known as POD modes, and they satisfy $\tilde{\mathbf{U}}^*\tilde{\mathbf{U}} = \mathbf{I}$. Similarly, columns of $\tilde{\mathbf{V}}$ are orthonormal and satisfy $\tilde{\mathbf{V}}^*\tilde{\mathbf{V}} = \mathbf{I}$.

Step 2. According to (48), the full matrix \mathbf{A} may be obtained by computing the pseudo-inverse of \mathbf{X} :

$$\mathbf{A} = \mathbf{X}'\tilde{\mathbf{V}}\tilde{\mathbf{\Sigma}}^{-1}\tilde{\mathbf{U}}^*. \quad (50)$$

However, we are only interested in the leading r eigenvalues and eigenvectors of \mathbf{A} , and we may thus project \mathbf{A} onto the POD modes in \mathbf{U} :

$$\tilde{\mathbf{A}} = \tilde{\mathbf{U}}^*\mathbf{A}\tilde{\mathbf{U}} = \tilde{\mathbf{U}}^*\mathbf{X}'\tilde{\mathbf{V}}\tilde{\mathbf{\Sigma}}^{-1}. \quad (51)$$

The key observation here is that the reduced matrix $\tilde{\mathbf{A}}$ has the same nonzero eigenvalues as the full matrix \mathbf{A} . Thus, we need only compute the reduced $\tilde{\mathbf{A}}$ directly, without ever working with the high-dimensional \mathbf{A} matrix. The reduced-order matrix $\tilde{\mathbf{A}}$ defines a linear model for the dynamics of the vector of POD coefficients $\tilde{\mathbf{x}}$:

$$\tilde{\mathbf{x}}_{k+1} = \tilde{\mathbf{A}}\tilde{\mathbf{x}}_k. \quad (52)$$

Note that the matrix $\tilde{\mathbf{U}}$ provides a map to reconstruct the full state \mathbf{x} from the reduced state $\tilde{\mathbf{x}}$: $\mathbf{x} = \tilde{\mathbf{U}}\tilde{\mathbf{x}}$.

Step 3. The spectral decomposition of $\tilde{\mathbf{A}}$ is computed:

$$\tilde{\mathbf{A}}\mathbf{W} = \mathbf{W}\mathbf{\Lambda}. \quad (53)$$

The entries of the diagonal matrix $\mathbf{\Lambda}$ are the DMD eigenvalues, which also correspond to eigenvalues of the full \mathbf{A} matrix. The columns of \mathbf{W} are eigenvectors of $\tilde{\mathbf{A}}$, and provide a coordinate transformation that diagonalizes the matrix. These columns may be thought of as linear combinations of POD mode amplitudes that behave linearly with a single temporal pattern given by λ .

Step 4. The high-dimensional DMD modes $\mathbf{\Phi}$ are reconstructed using the eigenvectors \mathbf{W} of the reduced system and the time-shifted snapshot matrix \mathbf{X}' according to:

$$\mathbf{\Phi} = \mathbf{X}'\tilde{\mathbf{V}}\tilde{\mathbf{\Sigma}}^{-1}\mathbf{W}. \quad (54)$$

Remarkably, these DMD modes are eigenvectors of the high-dimensional \mathbf{A} matrix corresponding to the eigenvalues in $\mathbf{\Lambda}$, as shown in Tu et al. [74]:

$$\begin{aligned} \mathbf{A}\mathbf{\Phi} &= (\mathbf{X}'\tilde{\mathbf{V}}\tilde{\mathbf{\Sigma}}^{-1}\tilde{\mathbf{U}}^*)\underbrace{(\mathbf{X}'\tilde{\mathbf{V}}\tilde{\mathbf{\Sigma}}^{-1}\mathbf{W})}_{\tilde{\mathbf{A}}} \\ &= \mathbf{X}'\tilde{\mathbf{V}}\tilde{\mathbf{\Sigma}}^{-1}\tilde{\mathbf{A}}\mathbf{W} \\ &= \mathbf{X}'\tilde{\mathbf{V}}\tilde{\mathbf{\Sigma}}^{-1}\mathbf{W}\mathbf{\Lambda} \\ &= \mathbf{\Phi}\mathbf{\Lambda}. \end{aligned}$$

In the original paper by Schmid [63], DMD modes are computed using $\Phi = \tilde{\mathbf{U}}\mathbf{W}$, which are known as *projected modes*; however, these modes are not guaranteed to be exact eigenvectors of \mathbf{A} . Because \mathbf{A} is defined as $\mathbf{A} = \mathbf{X}'\mathbf{X}^\dagger$, eigenvectors of \mathbf{A} should be in the column space of \mathbf{X}' , as in the exact DMD definition, instead of the column space of \mathbf{X} in the original DMD algorithm. In practice, the column spaces of \mathbf{X} and \mathbf{X}' will tend to be nearly identical for dynamical systems with low-rank structure, so that the projected and exact DMD modes often converge.

To find a DMD mode corresponding to a zero eigenvalue, $\lambda = 0$, it is possible to use the exact formulation if $\phi = \mathbf{X}'\tilde{\mathbf{V}}\tilde{\Sigma}^{-1}\mathbf{w} \neq 0$. However, if this expression is null, then the projected mode $\phi = \tilde{\mathbf{U}}\mathbf{w}$ should be used.

Historical perspective

In the original formulation, the snapshot matrices \mathbf{X} and \mathbf{X}' were formed with a collection of sequential snapshots, evenly spaced in time:

$$\mathbf{X} = \begin{bmatrix} | & | & \cdots & | \\ \mathbf{x}_1 & \mathbf{x}_2 & \cdots & \mathbf{x}_m \\ | & | & \cdots & | \end{bmatrix} \quad (55a)$$

$$\mathbf{X}' = \begin{bmatrix} | & | & \cdots & | \\ \mathbf{x}_2 & \mathbf{x}_3 & \cdots & \mathbf{x}_{m+1} \\ | & | & \cdots & | \end{bmatrix}. \quad (55b)$$

Thus, the matrix \mathbf{X} can be written in terms of iterations of the matrix \mathbf{A} as:

$$\mathbf{X} \approx \begin{bmatrix} | & | & \cdots & | \\ \mathbf{x}_1 & \mathbf{A}\mathbf{x}_1 & \cdots & \mathbf{A}^{m-1}\mathbf{x}_1 \\ | & | & \cdots & | \end{bmatrix}. \quad (56)$$

Thus, the columns of the matrix \mathbf{X} belong to a Krylov subspace generated by the propagator \mathbf{A} and the initial condition \mathbf{x}_1 . In addition, the matrix \mathbf{X}' may be related to \mathbf{X} through the *shift* operator as:

$$\mathbf{X}' = \mathbf{X}\mathbf{S}, \quad (57)$$

where \mathbf{S} is defined as

$$\mathbf{S} = \begin{bmatrix} 0 & 0 & 0 & \cdots & 0 & a_1 \\ 1 & 0 & 0 & \cdots & 0 & a_2 \\ 0 & 1 & 0 & \cdots & 0 & a_3 \\ \vdots & \vdots & \vdots & \ddots & \vdots & \vdots \\ 0 & 0 & 0 & \cdots & 1 & a_m \end{bmatrix}. \quad (58)$$

Thus, the first $m - 1$ columns of \mathbf{X}' are obtained directly by shifting the corresponding columns of \mathbf{X} , and the last column is obtained as a best-fit combination of the m columns of \mathbf{X} that minimizes the residual. In this way, the DMD algorithm resembles an Arnoldi algorithm used to find the dominant eigenvalues and eigenvectors

of a matrix \mathbf{A} through iteration. The matrix \mathbf{S} will share eigenvalues with the high-dimensional \mathbf{A} matrix, so that decomposition of \mathbf{S} may be used to obtain dynamic modes and eigenvalues. However, computations based on \mathbf{S} is not as numerically stable as the exact algorithm above.

Spectral decomposition and DMD expansion

One of the most important aspects of the DMD is the ability to expand the system state in terms of a data-driven spectral decomposition:

$$\mathbf{x}_k = \sum_{j=1}^r \phi_j \lambda_j^{k-1} b_j = \Phi \Lambda^{k-1} \mathbf{b}, \quad (59)$$

where ϕ_j are DMD modes (eigenvectors of the \mathbf{A} matrix), λ_j are DMD eigenvalues (eigenvalues of the \mathbf{A} matrix), and b_j is the mode amplitude. The vector \mathbf{b} of mode amplitudes is generally computed as

$$\mathbf{b} = \Phi^\dagger \mathbf{x}_1. \quad (60)$$

More principled approaches to select dominant and sparse modes have been considered [21, 26]. However, computing the mode amplitudes is generally quite expensive, even using the straightforward definition in (60). Instead, it is possible to compute these amplitudes using POD projected data:

$$\mathbf{x}_1 = \Phi \mathbf{b} \quad (61a)$$

$$\implies \tilde{\mathbf{U}} \tilde{\mathbf{x}}_1 = \mathbf{X}' \tilde{\mathbf{V}} \tilde{\Sigma}^{-1} \mathbf{W} \mathbf{b} \quad (61b)$$

$$\implies \tilde{\mathbf{x}}_1 = \tilde{\mathbf{U}}^* \mathbf{X}' \tilde{\mathbf{V}} \tilde{\Sigma}^{-1} \mathbf{W} \mathbf{b} \quad (61c)$$

$$\implies \tilde{\mathbf{x}}_1 = \tilde{\mathbf{A}} \mathbf{W} \mathbf{b} \quad (61d)$$

$$\implies \tilde{\mathbf{x}}_1 = \mathbf{W} \Lambda \mathbf{b} \quad (61e)$$

$$\implies \mathbf{b} = (\mathbf{W} \Lambda)^{-1} \tilde{\mathbf{x}}_1. \quad (61f)$$

The matrices \mathbf{W} and Λ are both size $r \times r$, as opposed to the large Φ matrix that is $n \times r$.

The spectral expansion above may also be written in continuous time by introducing the continuous eigenvalues $\omega = \log(\lambda)/\Delta t$:

$$\mathbf{x}(t) = \sum_{j=1}^r \phi_j e^{\omega_j t} b_j = \Phi \exp(\Omega t) \mathbf{b}, \quad (62)$$

where Ω is a diagonal matrix containing the continuous-time eigenvalues ω_j .

3.3 Extended DMD

The extended DMD algorithm [76] is essentially the same as standard DMD [74], except that instead of performing regression on direct measurements of the state, regression is performed on an augmented vector containing nonlinear measurements of the state.

As discussed earlier, eDMD is equivalent to the variational approach of conformation dynamics [51, 53, 54], which was developed in 2013 by Noé and Nüske.

Here, we will modify the notation slightly to conform to related methods. In eDMD, an augmented state is constructed:

$$\mathbf{y} = \Theta^T(\mathbf{x}) = \begin{bmatrix} \theta_1(\mathbf{x}) \\ \theta_2(\mathbf{x}) \\ \vdots \\ \theta_p(\mathbf{x}) \end{bmatrix}. \quad (63)$$

Θ may contain the original state \mathbf{x} as well as nonlinear measurements, so often $p \gg n$. Next, two data matrices are constructed, as in DMD:

$$\mathbf{Y} = \begin{bmatrix} | & | & & | \\ \mathbf{y}_1 & \mathbf{y}_2 & \cdots & \mathbf{y}_m \\ | & | & & | \end{bmatrix}, \quad \mathbf{Y}' = \begin{bmatrix} | & | & & | \\ \mathbf{y}_2 & \mathbf{y}_3 & \cdots & \mathbf{y}_{m+1} \\ | & | & & | \end{bmatrix}. \quad (64a)$$

Finally, a best-fit linear operator \mathbf{A}_Y is constructed that maps \mathbf{Y} into \mathbf{Y}' :

$$\mathbf{A}_Y = \operatorname{argmin}_{\mathbf{A}_Y} \|\mathbf{Y}' - \mathbf{A}_Y \mathbf{Y}\| = \mathbf{Y}' \mathbf{Y}^\dagger. \quad (65)$$

This regression may be written in terms of the data matrices $\Theta(\mathbf{X})$ and $\Theta(\mathbf{X}')$:

$$\mathbf{A}_Y = \operatorname{argmin}_{\mathbf{A}_Y} \|\Theta^T(\mathbf{X}') - \mathbf{A}_Y \Theta^T(\mathbf{X})\| = \Theta^T(\mathbf{X}') (\Theta^T(\mathbf{X}))^\dagger. \quad (66)$$

Because the augmented vector \mathbf{y} may be significantly larger than the state \mathbf{x} , kernel methods are often employed to compute this regression [77]. In principle, the enriched library Θ provides a larger basis in which to approximate the Koopman operator. It has been shown recently that in the limit of infinite snapshots, the extended DMD operator converges to the Koopman operator projected onto the subspace spanned by Θ [33]. However, if Θ does not span a Koopman invariant subspace, then the projected operator may not have any resemblance to the original Koopman operator, as all of the eigenvalues and eigenvectors may be different. In fact, it was shown that the extended DMD operator will have spurious eigenvalues and eigenvectors unless it is represented in terms of a Koopman invariant subspace [11]. Therefore, it is essential to use validation and cross-validation techniques to ensure that eDMD models are not overfit, as discussed below. For example, it was shown that eDMD cannot contain the original state \mathbf{x} as a measurement and represent a system that has multiple fixed points, periodic orbits, or other attractors, because these systems cannot be topologically conjugate to a finite-dimensional linear system [11].

3.4 Approximating Koopman eigenfunctions from data

In discrete-time, a Koopman eigenfunction $\varphi(\mathbf{x})$ evaluated at a number of data points in \mathbf{X} will satisfy:

$$\begin{bmatrix} \lambda\varphi(\mathbf{x}_1) \\ \lambda\varphi(\mathbf{x}_2) \\ \vdots \\ \lambda\varphi(\mathbf{x}_m) \end{bmatrix} = \begin{bmatrix} \varphi(\mathbf{x}_2) \\ \varphi(\mathbf{x}_3) \\ \vdots \\ \varphi(\mathbf{x}_{m+1}) \end{bmatrix}. \quad (67)$$

It is possible to approximate this eigenfunction as an expansion in terms of a set of candidate functions,

$$\Theta(\mathbf{x}) = [\theta_1(\mathbf{x}) \quad \theta_2(\mathbf{x}) \quad \cdots \quad \theta_p(\mathbf{x})]. \quad (68)$$

The Koopman eigenfunction may be approximated in this basis as:

$$\varphi(\mathbf{x}) \approx \sum_{k=1}^p \theta_k(\mathbf{x})\xi_k = \Theta(\mathbf{x})\boldsymbol{\xi}. \quad (69)$$

Writing (67) in terms of this expansion yields the matrix system:

$$(\lambda\Theta(\mathbf{X}) - \Theta(\mathbf{X}'))\boldsymbol{\xi} = \mathbf{0}. \quad (70)$$

If we seek the best *least-squares* fit to (70), this reduces to the extended DMD [77, 76] formulation:

$$\lambda\boldsymbol{\xi} = \Theta(\mathbf{X})^\dagger\Theta(\mathbf{X}')\boldsymbol{\xi}. \quad (71)$$

Note that (71) is the transpose of (66), so that left eigenvectors become right eigenvectors. Thus, eigenvectors $\boldsymbol{\xi}$ of $\Theta^\dagger\Theta'$ yield the coefficients of the eigenfunction $\varphi(\mathbf{x})$ represented in the basis $\Theta(\mathbf{x})$. It is absolutely essential to then confirm that predicted eigenfunctions actually behave linearly on trajectories, by comparing them with the predicted dynamics $\varphi_{k+1} = \lambda\varphi_k$, because the regression above will result in spurious eigenvalues and eigenvectors unless the basis elements θ_j span a Koopman invariant subspace [11].

Sparse identification of eigenfunctions

It is possible to leverage the SINDy regression [13] to identify Koopman eigenfunctions corresponding to a particular eigenvalue λ , selecting only the few active terms in the library $\Theta(\mathbf{x})$ to avoid overfitting. Given the data matrices, \mathbf{X} and $\dot{\mathbf{X}}$ from above it is possible to construct the library of basis functions $\Theta(\mathbf{X})$ as well as a library of directional derivatives, representing the possible terms in $\nabla\varphi(\mathbf{x}) \cdot \dot{\mathbf{x}}$ from (20):

$$\Gamma(\mathbf{x}, \dot{\mathbf{x}}) = [\nabla\theta_1(\mathbf{x}) \cdot \dot{\mathbf{x}} \quad \nabla\theta_2(\mathbf{x}) \cdot \dot{\mathbf{x}} \quad \cdots \quad \nabla\theta_p(\mathbf{x}) \cdot \dot{\mathbf{x}}]. \quad (72)$$

It is then possible to construct Γ from data:

$$\Gamma(\mathbf{X}, \dot{\mathbf{X}}) = \begin{bmatrix} \nabla\theta_1(\mathbf{x}_1) \cdot \dot{\mathbf{x}}_1 & \nabla\theta_2(\mathbf{x}_1) \cdot \dot{\mathbf{x}}_1 & \cdots & \nabla\theta_p(\mathbf{x}_1) \cdot \dot{\mathbf{x}}_1 \\ \nabla\theta_1(\mathbf{x}_2) \cdot \dot{\mathbf{x}}_2 & \nabla\theta_2(\mathbf{x}_2) \cdot \dot{\mathbf{x}}_2 & \cdots & \nabla\theta_p(\mathbf{x}_2) \cdot \dot{\mathbf{x}}_2 \\ \vdots & \vdots & \ddots & \vdots \\ \nabla\theta_1(\mathbf{x}_m) \cdot \dot{\mathbf{x}}_m & \nabla\theta_2(\mathbf{x}_m) \cdot \dot{\mathbf{x}}_m & \cdots & \nabla\theta_p(\mathbf{x}_m) \cdot \dot{\mathbf{x}}_m \end{bmatrix}.$$

For a given eigenvalue λ , the Koopman PDE in (20) may be evaluated on data:

$$\left(\lambda\Theta(\mathbf{X}) - \Gamma(\mathbf{X}, \dot{\mathbf{X}})\right)\xi = \mathbf{0}. \quad (73)$$

The formulation in (73) is implicit, so that ξ will be in the null-space of $\lambda\Theta(\mathbf{X}) - \Gamma(\mathbf{X}, \dot{\mathbf{X}})$. The right null-space of (73) for a given λ is spanned by the right singular vectors of $\lambda\Theta(\mathbf{X}) - \Gamma(\mathbf{X}, \dot{\mathbf{X}}) = \mathbf{U}\Sigma\mathbf{V}^*$ (i.e., columns of \mathbf{V}) corresponding to zero-valued singular values. It may be possible to identify the few active terms in an eigenfunction by finding the sparsest vector in the null-space [60], as in the implicit-SINDy algorithm [41] described in Sec. ?? . In this formulation, the eigenvalues λ are not known *a priori*, and must be learned with the approximate eigenfunction. Koopman eigenfunctions and eigenvalues can also be determined as the solution to the eigenvalue problem $\mathbf{A}_Y\xi_\alpha = \lambda_\alpha\xi_\alpha$, where $\mathbf{A}_Y = \Theta^\dagger\Gamma$ is obtained via least-squares regression, as in the continuous-time version of eDMD. While many eigenfunctions are spurious, those corresponding to lightly damped eigenvalues can be well approximated.

From a practical standpoint, data in \mathbf{X} does not need to be sampled from full trajectories, but can be obtained using more sophisticated strategies such as latin hypercube sampling or sampling from a distribution over the phase space. Moreover, reproducing kernel Hilbert spaces (RKHS) can be employed to describe $\varphi(\mathbf{x})$ *locally* in patches of state space.

Example: Duffing system (Kaiser et al [28]). We demonstrate the sparse identification of Koopman eigenfunctions on the undamped Duffing oscillator:

$$\frac{d}{dt} \begin{bmatrix} x_1 \\ x_2 \end{bmatrix} = \begin{bmatrix} x_2 \\ x_1 - x_1^3 \end{bmatrix}$$

where x_1 is the position and x_2 is the velocity of a particle in a double well potential with equilibria $(0, 0)$ and $(\pm 1, 0)$. This system is conservative, with Hamiltonian $\mathcal{H} = \frac{1}{2}x_2^2 - \frac{1}{2}x_1^2 + \frac{1}{4}x_1^4$. The Hamiltonian, and in general any conserved quantity, is a Koopman eigenfunction with zero eigenvalue.

For the eigenvalue $\lambda = 0$, (73) becomes $-\Gamma(\mathbf{X}, \dot{\mathbf{X}})\xi = \mathbf{0}$, and hence a sparse ξ is sought in the null-space of $-\Gamma(\mathbf{X}, \dot{\mathbf{X}})$. A library of candidate functions is constructed from data, employing polynomials up to fourth order:

$$\Theta(\mathbf{X}) = \begin{bmatrix} | & | & | & | & \cdots & | \\ x_1(t) & x_2(t) & x_1^2(t) & x_1(t)x_2(t) & \cdots & x_2^4(t) \\ | & | & | & | & & | \end{bmatrix}$$

and

$$\Gamma(\mathbf{X}, \dot{\mathbf{X}}) = \begin{bmatrix} | & | & | & | & \cdots & | \\ \dot{x}_1(t) & \dot{x}_2(t) & 2x_1(t)\dot{x}_1(t) & x_2(t)\dot{x}_1(t) + x_1(t)\dot{x}_2(t) & \cdots & 4x_2(t)^3\dot{x}_2(t) \\ | & | & | & | & & | \end{bmatrix}.$$

A sparse vector of coefficients ξ may be identified, with the few non-zero entries determining the active terms in the Koopman eigenfunction. The identified Koopman eigenfunction associated with $\lambda = 0$ is

$$\varphi(\mathbf{x}) = -2/3x_1^2 + 2/3x_2^2 + 1/3x_1^4. \quad (74)$$

This eigenfunction matches the Hamiltonian perfectly up to a constant scaling.

3.5 Data-driven Koopman and delay coordinates

Instead of advancing instantaneous linear or nonlinear measurements of the state of a system directly, as in DMD, it may be possible to obtain intrinsic measurement coordinates for Koopman based on time-delayed measurements of the system [69, 10, 3, 22]. This perspective is data-driven, relying on the wealth of information from previous measurements to inform the future. Unlike a linear or weakly nonlinear system, where trajectories may get trapped at fixed points or on periodic orbits, chaotic dynamics are particularly well-suited to this analysis: trajectories evolve to densely fill an attractor, so more data provides more information. The use of delay coordinates may be especially important for systems with long-term memory effects, where the Koopman approach has recently been shown to provide a successful analysis tool [70]. Interestingly, a connection between the Koopman operator and the Takens embedding was explored as early as 2004 [47], where a stochastic Koopman operator is defined and a statistical Takens theorem is proven.

The time-delay measurement scheme is shown schematically in Fig. 3, as illustrated on the Lorenz system for a single time-series measurement of the first variable, $x(t)$. The conditions of the Takens embedding theorem are satisfied [73], so it is possible to obtain a diffeomorphism between a delay embedded attractor and the attractor in the original coordinates. We then obtain eigen-time-delay coordinates from a time-series of a single measurement $x(t)$ by taking the SVD of the Hankel matrix \mathbf{H} :

$$\mathbf{H} = \begin{bmatrix} x(t_1) & x(t_2) & \cdots & x(t_{m_c}) \\ x(t_2) & x(t_3) & \cdots & x(t_{m_c+1}) \\ \vdots & \vdots & \ddots & \vdots \\ x(t_{m_o}) & x(t_{m_o+1}) & \cdots & x(t_m) \end{bmatrix} = \mathbf{U}\mathbf{\Sigma}\mathbf{V}^*. \quad (75)$$

The columns of \mathbf{U} and \mathbf{V} from the SVD are arranged hierarchically by their ability to model the columns and rows of \mathbf{H} , respectively. Often, \mathbf{H} may admit a low-rank approximation by the first r columns of \mathbf{U} and \mathbf{V} . Note that the Hankel matrix in (75) is the basis of the eigensystem realization algorithm [27] in linear system identification and singular spectrum analysis (SSA) [9] in climate time-series analysis.

The low-rank approximation to (75) provides a *data-driven* measurement system that is approximately invariant to the Koopman operator for states on the attractor. By definition, the dynamics map the attractor into itself, making it *invariant* to the flow. In other words, the columns of \mathbf{U} form a Koopman invariant subspace. We may re-write (75) with the Koopman operator $\mathcal{K} \triangleq \mathcal{K}_{\Delta t}$:

$$\mathbf{H} = \begin{bmatrix} x(t_1) & \mathcal{K}x(t_1) & \cdots & \mathcal{K}^{m_c-1}x(t_1) \\ \mathcal{K}x(t_1) & \mathcal{K}^2x(t_1) & \cdots & \mathcal{K}^{m_c}x(t_1) \\ \vdots & \vdots & \ddots & \vdots \\ \mathcal{K}^{m_o-1}x(t_1) & \mathcal{K}^{m_o}x(t_1) & \cdots & \mathcal{K}^{m-1}x(t_1) \end{bmatrix}. \quad (76)$$

The columns of (75) are well-approximated by the first r columns of \mathbf{U} . The first r columns of \mathbf{V} provide a time series of the magnitude of each of the columns of $\mathbf{U}\mathbf{\Sigma}$ in the data. By plotting the first three columns of \mathbf{V} , we obtain an embedded attractor for the Lorenz system (See Fig. 3).

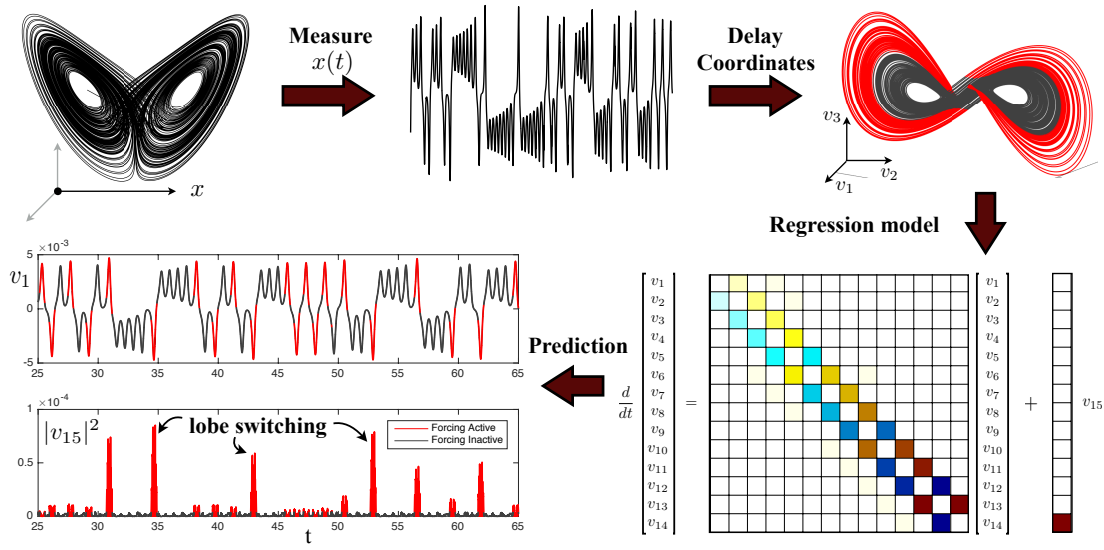


Figure 3: Decomposition of chaos into a linear system with forcing. A time series $x(t)$ is stacked into a Hankel matrix \mathbf{H} . The SVD of \mathbf{H} yields a hierarchy of *eigen* time series that produce a delay-embedded attractor. A best-fit linear regression model is obtained on the delay coordinates \mathbf{v} ; the linear fit for the first $r - 1$ variables is excellent, but the last coordinate v_r is not well-modeled as linear. Instead, v_r is an input that forces the first $r - 1$ variables. Rare forcing events correspond to lobe switching in the chaotic dynamics. This architecture is called the Hankel alternative view of Koopman (HAVOK) analysis, from [10]. *Figure modified from Brunton et al. [10].*

The connection between eigen-time-delay coordinates from (75) and the Koopman operator motivates a linear regression model on the variables in \mathbf{V} . Even with an approximately Koopman-invariant measurement system, there remain challenges to identifying a linear model for a chaotic system. A linear model, however detailed, cannot capture multiple fixed points or the unpredictable behavior characteristic of chaos with a positive Lyapunov exponent [11]. Instead of constructing a closed linear model for the first r variables in \mathbf{V} , we build a linear model on the first $r - 1$ variables and recast the last variable, v_r , as a forcing term:

$$\frac{d}{dt}\mathbf{v}(t) = \mathbf{A}\mathbf{v}(t) + \mathbf{B}v_r(t), \quad (77)$$

where $\mathbf{v} = [v_1 \ v_2 \ \cdots \ v_{r-1}]^T$ is a vector of the first $r - 1$ eigen-time-delay coordinates. Other work has investigated the splitting of dynamics into deterministic linear, and chaotic stochastic dynamics [44].

In all of the examples explored in [10], the linear model on the first $r - 1$ terms is accurate, while no linear model represents v_r . Instead, v_r is an input forcing to the linear dynamics in (77), which approximates the nonlinear dynamics. The statistics of $v_r(t)$ are non-Gaussian, with long tails correspond to rare-event forcing that drives lobe switching in the Lorenz system; this is related to rare-event forcing distributions

observed and modeled by others [39, 62, 40]. The forced linear system in (77) was discovered after applying the SINDy algorithm [13] to delay coordinates of the Lorenz system. Continuing to develop Koopman on delay coordinates has significant promise in the context of closed-loop feedback control, where it may be possible to manipulate the behavior of a chaotic system by treating v_r as a disturbance.

In addition, the use of delay coordinates as intrinsic measurements for Koopman analysis suggests that Koopman theory may also be used to improve spatially distributed sensor technologies. A spatial array of sensors, for example the $\mathcal{O}(100)$ strain sensors on the wings of flying insects, may use phase delay coordinates to provide nearly optimal embeddings to detect and control convective structures (e.g., stall from a gust, leading edge vortex formation and convection, etc.).

3.6 Neural networks for Koopman embeddings

Despite the promise of Koopman embeddings, obtaining tractable representations has remained a central challenge. Recall that even for relatively simple dynamical systems, the eigenfunctions of the Koopman operator may be arbitrarily complex. Deep learning, which is well-suited for representing arbitrary functions, has recently emerged as a promising approach for discovering and representing Koopman eigenfunctions [75, 42, 72, 78, 55, 37, 38], providing a data-driven embedding of strongly nonlinear systems into intrinsic linear coordinates. In particular, the Koopman perspective fits naturally with the deep auto-encoder structure, where a few key latent variables $\mathbf{y} = \varphi(\mathbf{x})$ are discovered to parameterize the dynamics. In a Koopman network, an additional constraint is enforced so that the dynamics must be linear on these latent variables, forcing the functions $\varphi(\mathbf{x})$ to be Koopman eigenfunctions, as illustrated in Fig. 4. The constraint of linear dynamics is enforced by the loss function $\|\varphi(\mathbf{x}_{k+1}) - \mathbf{K}\varphi(\mathbf{x}_k)\|$, where \mathbf{K} is a matrix. In general, linearity is enforced over multiple time steps, so that a trajectory is captured by iterating \mathbf{K} on the latent variables. In addition, it is important to be able to map back to physical variables \mathbf{x} , which is why the autoencoder structure is favorable [38]. Variational autoencoders are also used for stochastic dynamical systems, such as molecular dynamics, where the map back to physical configuration space from the latent variables is probabilistic [75, 42].

For simple systems with a discrete eigenvalue spectrum, a compact representation may be obtained in terms of a few autoencoder variables. However, dynamical systems with continuous eigenvalue spectra defy low-dimensional representations using many existing neural network or Koopman representations. Continuous spectrum dynamics are ubiquitous, ranging from the simple pendulum to nonlinear optics and broadband turbulence. For example, the classical pendulum, given by

$$\ddot{x} = -\sin(\omega x) \quad (78)$$

exhibits a continuous range of frequencies, from ω to 0, as the amplitude of the pendulum oscillation is increased. Thus, the continuous spectrum confounds a simple description in terms of a few Koopman eigenfunctions [46]. Indeed, away from the linear regime, an infinite Fourier sum is required to approximate the shift in frequency.

In a recent work by Lusch et al. [38], an auxiliary network is used to parameterize

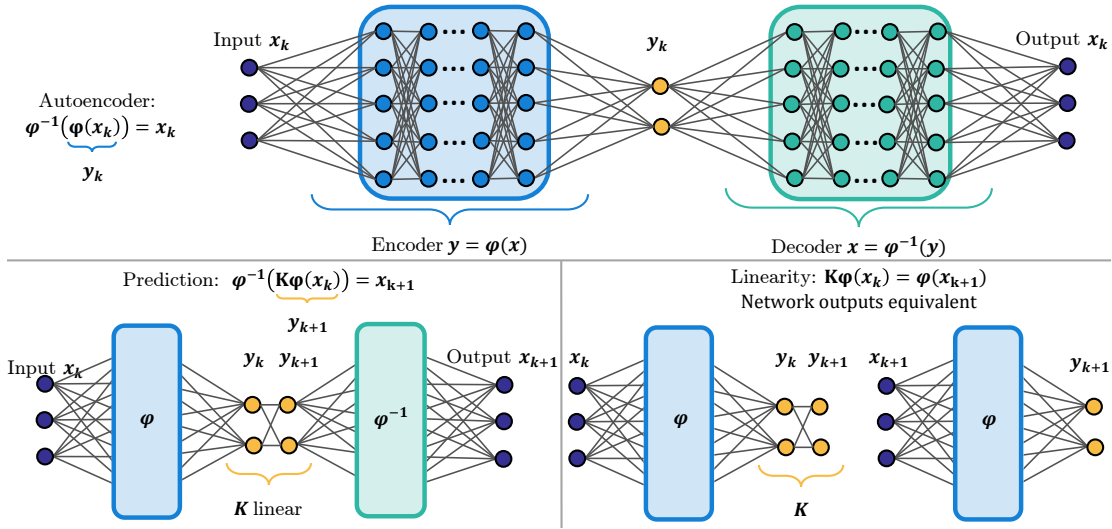


Figure 4: Deep neural network architecture used to identify Koopman eigenfunctions $\varphi(x)$. The network is based on a deep auto-encoder (a), which identifies intrinsic coordinates $y = \varphi(x)$. Additional loss functions are included to enforce linear dynamics in the auto-encoder variables (b,c). *Reproduced with permission from Lusch et al. [38].*

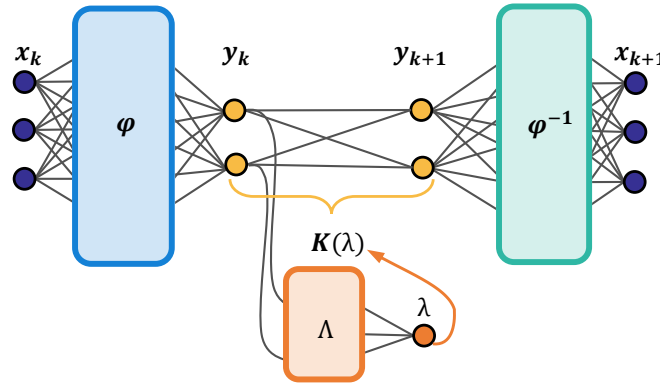


Figure 5: Modified network architecture with auxiliary network to parameterize the continuous eigenvalue spectrum. A continuous eigenvalue λ enables aggressive dimensionality reduction in the auto-encoder, avoiding the need for higher harmonics of the fundamental frequency that are generated by the nonlinearity. *Reproduced with permission from Lusch et al. [38].*

the continuously varying eigenvalue, enabling a network structure that is both parsimonious and interpretable. This parameterized network is depicted schematically in Fig. 5 and illustrated on the simple pendulum in Fig. 6. In contrast to other network structures, which require a large autoencoder layer to encode the continuous frequency shift with an asymptotic expansion in terms of harmonics of the natural frequency, the parameterized network is able to identify a single complex conjugate pair of eigenfunctions with a varying imaginary eigenvalue pair. If this explicit frequency dependence is unaccounted for, then a high-dimensional network is necessary to account for the shifting frequency and eigenvalues.

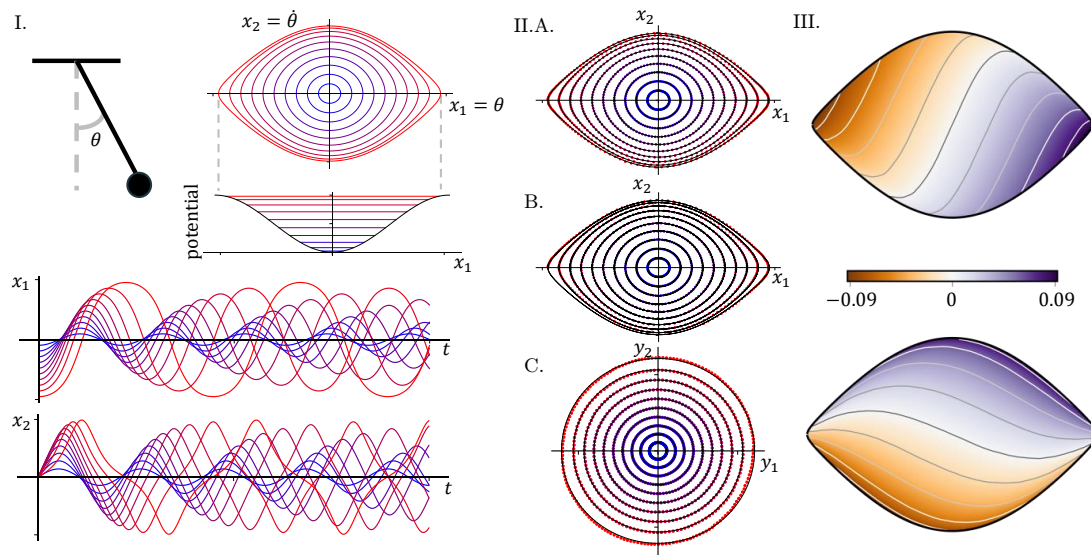


Figure 6: Neural network embedding of the nonlinear pendulum, using the parameterized network in Fig. 5. As the pendulum amplitude increases, the frequency continuously changes (I). In the Koopman eigenfunction coordinates (III), the dynamics become linear, given by perfect circles (IIIC). *Reproduced with permission from Lusch et al. [38].*

It is expected that neural network representations of dynamical systems, and Koopman embeddings in particular, will remain a growing area of interest in data-driven dynamics. Combining the representational power of deep learning with the elegance and simplicity of Koopman embeddings has the potential to transform the analysis and control of complex systems.

4 Koopman control

4.1 Nonlinear system identification for control

The data-driven modeling and control of complex systems is undergoing a revolution, driven by the rise of big data, advanced algorithms in machine learning and optimization, and modern computational hardware. Despite the increasing use of equation-free and adaptive control methods, there remains a wealth of powerful model-based control techniques, such as linear optimal control and model predictive control (MPC) [23, 17]. Increasingly, these model-based control strategies are aided by data-driven techniques that characterize the input–output dynamics of a system of interest from measurements alone, without relying on first principles modeling. Broadly speaking, this is known as *system identification*, which has a long and rich history in control theory going back decades to the time of Kalman. However, with increasingly powerful data-driven techniques, nonlinear system identification is the focus of renewed interest.

The goal of system identification is to identify a low-order model of the input–output dynamics from actuation \mathbf{u} to measurements \mathbf{y} . If we are able to measure the full state \mathbf{x} of the system, then this reduces to identifying the dynamics \mathbf{f} that satisfy:

$$\frac{d}{dt}\mathbf{x} = \mathbf{f}(\mathbf{x}, \mathbf{u}). \quad (79)$$

This problem may be formulated in discrete-time, since data is typically collected at discrete instances in time and control laws are often implemented digitally. In this case, the dynamics read:

$$\mathbf{x}_{k+1} = \mathbf{F}(\mathbf{x}_k, \mathbf{u}_k). \quad (80)$$

When the dynamics are approximately linear, we may identify a linear system

$$\mathbf{x}_{k+1} = \mathbf{A}\mathbf{x}_k + \mathbf{B}\mathbf{u}_k, \quad (81)$$

which is the approach taken in the DMD with control (DMDc) algorithm below.

It may also be advantageous to identify a set of measurements $\mathbf{y} = \mathbf{g}(\mathbf{x})$, in which the unforced nonlinear dynamics appear linear:

$$\mathbf{y}_{k+1} = \mathbf{A}_Y\mathbf{y}_k. \quad (82)$$

This is the approach taken in the Koopman control method below. In this way, nonlinear dynamics may be estimated and controlled using standard textbook linear control theory in the intrinsic coordinates \mathbf{y} [32, 28].

Finally, the nonlinear dynamics in (79) or (80) may be identified directly using the SINDY with control algorithm. The resulting models may be used with model predictive control for the control of fully nonlinear systems [29].

4.2 DMD with control

Proctor et al. [58] extended the DMD algorithm to include the effect of actuation and control, in the so-called DMD with control (DMDc) algorithm. It was observed that

naively applying DMD to data from a system with actuation would often result in incorrect dynamics, as the effects of internal dynamics are confused with the effects of actuation. DMDc was originally motivated by the problem of characterizing and controlling the spread of disease, where it is unreasonable to stop intervention efforts (e.g., vaccinations) just to obtain a characterization of the unforced dynamics [59]. Instead, if the actuation signal is measured, a new DMD regression may be formulated in order to disambiguate the effect of internal dynamics from that of actuation and control. Subsequently, this approach has been extended to perform DMDc on heavily subsampled or compressed measurements by Bai et al. [5].

The DMDc method seeks to identify the best-fit linear operators \mathbf{A} and \mathbf{B} that approximately satisfy the following dynamics on measurement data:

$$\mathbf{x}_{k+1} \approx \mathbf{A}\mathbf{x}_k + \mathbf{B}\mathbf{u}_k. \quad (83)$$

In addition to the snapshot matrix $\mathbf{X} = [\mathbf{x}_1 \ \mathbf{x}_2 \ \cdots \ \mathbf{x}_m]$ and the time-shifted snapshot matrix $\mathbf{X}' = [\mathbf{x}_2 \ \mathbf{x}_3 \ \cdots \ \mathbf{x}_{m+1}]$ from (55), a matrix of the actuation input history is assembled:

$$\mathbf{\Upsilon} = \begin{bmatrix} | & | & \cdots & | \\ \mathbf{u}_1 & \mathbf{u}_2 & \cdots & \mathbf{u}_m \\ | & | & \cdots & | \end{bmatrix}. \quad (84)$$

The dynamics in (83) may be written in terms of the data matrices:

$$\mathbf{X}' \approx \mathbf{A}\mathbf{X} + \mathbf{B}\mathbf{\Upsilon}. \quad (85)$$

As in the DMD algorithm (see Sec. 3.1), the leading eigenvalues and eigenvectors of the best-fit linear operator \mathbf{A} are obtained via dimensionality reduction and regression. If the actuation matrix \mathbf{B} is known, then it is straightforward to correct for the actuation and identify the spectral decomposition of \mathbf{A} by replacing \mathbf{X}' with $\mathbf{X}' - \mathbf{B}\mathbf{\Upsilon}$ in the DMD algorithm:

$$(\mathbf{X}' - \mathbf{B}\mathbf{\Upsilon}) \approx \mathbf{A}\mathbf{X}. \quad (86)$$

When \mathbf{B} is unknown, both \mathbf{A} and \mathbf{B} must be simultaneously identified. In this case, the dynamics in (85) may be recast as:

$$\mathbf{X}' \approx [\mathbf{A} \ \mathbf{B}] \begin{bmatrix} \mathbf{X} \\ \mathbf{\Upsilon} \end{bmatrix} = \mathbf{G}\mathbf{\Omega}, \quad (87)$$

and the matrix $\mathbf{G} = [\mathbf{A} \ \mathbf{B}]$ is obtained via least-squares regression:

$$\mathbf{G} \approx \mathbf{X}'\mathbf{\Omega}^\dagger. \quad (88)$$

The matrix $\mathbf{\Omega} = [\mathbf{X}^* \ \mathbf{\Upsilon}^*]^*$ is generally a high-dimensional data matrix, which may be approximated using the SVD:

$$\mathbf{\Omega} = \tilde{\mathbf{U}}\tilde{\mathbf{\Sigma}}\tilde{\mathbf{V}}^*. \quad (89)$$

The matrix $\tilde{\mathbf{U}}$ must be split into two matrices, $\tilde{\mathbf{U}} = [\tilde{\mathbf{U}}_1^* \quad \tilde{\mathbf{U}}_2^*]^*$, to provide bases for \mathbf{X} and \mathbf{Y} . Unlike the DMD algorithm, $\tilde{\mathbf{U}}$ provides a reduced basis for the *input space*, while $\hat{\mathbf{U}}$ from

$$\mathbf{X}' = \hat{\mathbf{U}}\hat{\Sigma}\hat{\mathbf{V}}^* \quad (90)$$

defines a reduced basis for the *output space*. It is then possible to approximate $\mathbf{G} = [\mathbf{A} \quad \mathbf{B}]$ by projecting onto this basis:

$$\tilde{\mathbf{G}} = \hat{\mathbf{U}}^*\mathbf{G} \begin{bmatrix} \hat{\mathbf{U}} \\ \mathbf{I} \end{bmatrix}. \quad (91)$$

The resulting projected matrices $\tilde{\mathbf{A}}$ and $\tilde{\mathbf{B}}$ in $\tilde{\mathbf{G}}$ are:

$$\tilde{\mathbf{A}} = \hat{\mathbf{U}}^*\mathbf{A}\hat{\mathbf{U}} = \hat{\mathbf{U}}^*\mathbf{X}'\tilde{\mathbf{V}}\tilde{\Sigma}^{-1}\tilde{\mathbf{U}}_1^*\hat{\mathbf{U}} \quad (92a)$$

$$\tilde{\mathbf{B}} = \hat{\mathbf{U}}^*\mathbf{B} = \hat{\mathbf{U}}^*\mathbf{X}'\tilde{\mathbf{V}}\tilde{\Sigma}^{-1}\tilde{\mathbf{U}}_2^*. \quad (92b)$$

More importantly, it is possible to recover the DMD eigenvectors Φ from the eigendecomposition $\tilde{\mathbf{A}}\mathbf{W} = \mathbf{W}\Lambda$:

$$\Phi = \mathbf{X}'\tilde{\mathbf{V}}\tilde{\Sigma}^{-1}\tilde{\mathbf{U}}_1^*\hat{\mathbf{U}}\mathbf{W}. \quad (93)$$

Ambiguity in identifying closed-loop systems

For systems that are being actively controlled via feedback, with $\mathbf{u} = \mathbf{K}\mathbf{x}$,

$$\mathbf{x}_{k+1} = \mathbf{A}\mathbf{x}_k + \mathbf{B}\mathbf{u}_k \quad (94a)$$

$$= \mathbf{A}\mathbf{x}_k + \mathbf{B}\mathbf{K}\mathbf{x}_k \quad (94b)$$

$$= (\mathbf{A} + \mathbf{B}\mathbf{K})\mathbf{x}_k, \quad (94c)$$

it is impossible to disambiguate the dynamics \mathbf{A} and the actuation $\mathbf{B}\mathbf{K}$. In this case, it is important to add perturbations to the actuation signal \mathbf{u} to provide additional information. These perturbations may be a white noise process or occasional impulses that provide a kick to the system, providing a signal to disambiguate the dynamics from the feedback signal.

4.3 Koopman operator nonlinear control

For nonlinear systems, it may be advantageous to identify data-driven coordinate transformations that make the dynamics appear linear. These coordinate transformations are related to *intrinsic* coordinates defined by eigenfunctions of the Koopman operator (see Sec. 2). Koopman analysis has thus been leveraged for nonlinear estimation [67, 68] and control [32, 28, 56].

It is possible to design estimators and controllers directly from DMD or eDMD models, and Korda et al. [32] used model predictive control (MPC) to control nonlinear systems with eDMD models. MPC performance is also surprisingly good for DMD models, as shown in Kaiser et al. [29]. In addition, Peitz et al. [56] demonstrated the

use of MPC for switching control between a small number of actuation values to track a reference value of lift in an unsteady fluid flow; for each constant actuation value, a separate eDMD model was characterized. Surana [67] and Surana and Banaszuk [68] have also demonstrated excellent nonlinear estimators based on Koopman Kalman filters. However, as discussed previously, eDMD models may contain many spurious eigenvalues and eigenvectors because of closure issues related to finding a Koopman-invariant subspace. Instead, it may be advantageous to identify a handful of relevant Koopman eigenfunctions and perform control directly in these coordinates [28].

In Sec. 3, we described several strategies to approximate Koopman eigenfunctions, $\varphi(\mathbf{x})$, where the dynamics become linear:

$$\frac{d}{dt}\varphi(\mathbf{x}) = \lambda\varphi(\mathbf{x}). \quad (95)$$

In Kaiser et al. [28] the Koopman eigenfunction equation was extended for control-affine nonlinear systems:

$$\frac{d}{dt}\mathbf{x} = \mathbf{f}(\mathbf{x}) + \mathbf{B}\mathbf{u}. \quad (96)$$

For these systems, it is possible to apply the chain rule to $\frac{d}{dt}\varphi(\mathbf{x})$, yielding:

$$\frac{d}{dt}\varphi(\mathbf{x}) = \nabla\varphi(\mathbf{x}) \cdot (\mathbf{f}(\mathbf{x}) + \mathbf{B}\mathbf{u}) \quad (97a)$$

$$= \lambda\varphi(\mathbf{x}) + \nabla\varphi(\mathbf{x}) \cdot \mathbf{B}\mathbf{u}. \quad (97b)$$

Note that even with actuation, the dynamics of Koopman eigenfunctions remain linear, and the effect of actuation is still additive. However, now the actuation mode $\nabla\varphi(\mathbf{x}) \cdot \mathbf{B}$ may be state dependent. In fact, the actuation *will* be state dependent unless the directional derivative of the eigenfunction is constant in the \mathbf{B} direction. Fortunately, there are many powerful generalizations of standard Riccati-based linear control theory (e.g., LQR, Kalman filters, etc.) for systems with a *state-dependent* Riccati equation.

References

- [1] R. Abraham and J. E. Marsden. *Foundations of mechanics*, volume 36. Benjamin/Cummings Publishing Company Reading, Massachusetts, 1978.
- [2] R. Abraham, J. E. Marsden, and T. Ratiu. *Manifolds, Tensor Analysis, and Applications*, volume 75 of *Applied Mathematical Sciences*. Springer-Verlag, 1988.
- [3] H. Arbabi and I. Mezić. Ergodic theory, dynamic mode decomposition and computation of spectral properties of the Koopman operator. *SIAM J. Appl. Dyn. Syst.*, 16(4):2096–2126, 2017.
- [4] T. Askham and J. N. Kutz. Variable projection methods for an optimized dynamic mode decomposition. *SIAM J. Appl. Dyn. Syst.*, 17(1):380–416, 2018.
- [5] Z. Bai, E. Kaiser, J. L. Proctor, J. N. Kutz, and S. L. Brunton. Dynamic mode decomposition for compressive system identification. *arXiv preprint arXiv:1710.07737*, 2017.
- [6] S. Banks. Infinite-dimensional Carleman linearization, the Lie series and optimal control of nonlinear partial differential equations. *International journal of systems science*, 23(5):663–675, 1992.
- [7] G. D. Birkhoff. Proof of the ergodic theorem. *Proceedings of the National Academy of Sciences*, 17(12):656–660, 1931.
- [8] G. D. Birkhoff and B. O. Koopman. Recent contributions to the ergodic theory. *Proceedings of the National Academy of Sciences*, 18(3):279–282, 1932.
- [9] D. Broomhead and R. Jones. Time-series analysis. In *Proceedings of the Royal Society of London A: Mathematical, Physical and Engineering Sciences*, volume 423, pages 103–121. The Royal Society, 1989.
- [10] S. L. Brunton, B. W. Brunton, J. L. Proctor, E. Kaiser, and J. N. Kutz. Chaos as an intermittently forced linear system. *Nature Communications*, 8(19):1–9, 2017.
- [11] S. L. Brunton, B. W. Brunton, J. L. Proctor, and J. N. Kutz. Koopman invariant subspaces and finite linear representations of nonlinear dynamical systems for control. *PLoS ONE*, 11(2):e0150171, 2016.
- [12] S. L. Brunton and J. N. Kutz. *Data-Driven Science and Engineering: Machine Learning, Dynamical Systems, and Control*. Cambridge University Press, 2019.
- [13] S. L. Brunton, J. L. Proctor, and J. N. Kutz. Discovering governing equations from data by sparse identification of nonlinear dynamical systems. *Proceedings of the National Academy of Sciences*, 113(15):3932–3937, 2016.
- [14] M. Budišić and I. Mezić. An approximate parametrization of the ergodic partition using time averaged observables. In *Decision and Control, 2009 held jointly with the 2009 28th Chinese Control Conference. CDC/CCC 2009. Proceedings of the 48th IEEE Conference on*, pages 3162–3168. IEEE, 2009.
- [15] M. Budišić and I. Mezić. Geometry of the ergodic quotient reveals coherent structures in flows. *Physica D: Nonlinear Phenomena*, 241(15):1255–1269, 2012.
- [16] M. Budišić, R. Mohr, and I. Mezić. Applied Koopmanism a). *Chaos: An Interdisciplinary Journal of Nonlinear Science*, 22(4):047510, 2012.
- [17] E. F. Camacho and C. B. Alba. *Model predictive control*. Springer Science & Business Media, 2013.
- [18] T. Carleman. Application de la théorie des équations intégrales linéaires aux systèmes d'équations différentielles non linéaires. *Acta Mathematica*, 59(1):63–87, 1932.
- [19] T. Carleman. Sur la théorie de l'équation intégrodifférentielle de boltzmann. *Acta Mathematica*, 60(1):91–146, 1933.
- [20] T. Carleman. Sur les systemes lineaires aux dérivées partielles du premier ordrea deux variables. *CR Acad. Sci. Paris*, 197:471–474, 1933.
- [21] K. K. Chen, J. H. Tu, and C. W. Rowley. Variants of dynamic mode decomposition: Boundary condition, Koopman, and Fourier analyses. *Journal of Nonlinear Science*, 22(6):887–915, 2012.
- [22] S. Das and D. Giannakis. Delay-coordinate maps and the spectra of Koopman operators. *arXiv preprint arXiv:1706.08544*, 2017.
- [23] C. E. Garcia, D. M. Prett, and M. Morari. Model predictive control: theory and practice—a survey. *Automatica*, 25(3):335–348, 1989.
- [24] M. Gavish and D. L. Donoho. The optimal hard threshold for singular values is $4/\sqrt{3}$. *IEEE Transactions on Information Theory*, 60(8):5040–5053, 2014.

- [25] P. Holmes and J. Guckenheimer. *Nonlinear oscillations, dynamical systems, and bifurcations of vector fields*, volume 42 of *Applied Mathematical Sciences*. Springer-Verlag, Berlin, Heidelberg, 1983.
- [26] M. R. Jovanović, P. J. Schmid, and J. W. Nichols. Sparsity-promoting dynamic mode decomposition. *Physics of Fluids*, 26(2):024103, 2014.
- [27] J. N. Juang and R. S. Pappa. An eigensystem realization algorithm for modal parameter identification and model reduction. *Journal of Guidance, Control, and Dynamics*, 8(5):620–627, 1985.
- [28] E. Kaiser, J. N. Kutz, and S. L. Brunton. Data-driven discovery of Koopman eigenfunctions for control. *arXiv preprint arXiv:1707.01146*, 2017.
- [29] E. Kaiser, J. N. Kutz, and S. L. Brunton. Sparse identification of nonlinear dynamics for model predictive control in the low-data limit. *Proceedings of the Royal Society of London A*, 474(2219), 2018.
- [30] B. O. Koopman. Hamiltonian systems and transformation in Hilbert space. *Proceedings of the National Academy of Sciences*, 17(5):315–318, 1931.
- [31] B. O. Koopman and J.-v. Neumann. Dynamical systems of continuous spectra. *Proceedings of the National Academy of Sciences of the United States of America*, 18(3):255, 1932.
- [32] M. Korda and I. Mezić. Linear predictors for nonlinear dynamical systems: Koopman operator meets model predictive control. *Automatica*, 93(149–160), 2018.
- [33] M. Korda and I. Mezić. On convergence of extended dynamic mode decomposition to the Koopman operator. *Journal of Nonlinear Science*, 28(2):687–710, 2018.
- [34] K. Kowalski, W.-H. Steeb, and K. Kowalksi. *Nonlinear dynamical systems and Carleman linearization*. World Scientific, 1991.
- [35] J. N. Kutz, S. L. Brunton, B. W. Brunton, and J. L. Proctor. *Dynamic Mode Decomposition: Data-Driven Modeling of Complex Systems*. SIAM, 2016.
- [36] Y. Lan and I. Mezić. Linearization in the large of nonlinear systems and Koopman operator spectrum. *Physica D: Nonlinear Phenomena*, 242(1):42–53, 2013.
- [37] Q. Li, F. Dietrich, E. M. Bollt, and I. G. Kevrekidis. Extended dynamic mode decomposition with dictionary learning: A data-driven adaptive spectral decomposition of the Koopman operator. *Chaos: An Interdisciplinary Journal of Nonlinear Science*, 27(10):103111, 2017.
- [38] B. Lusch, J. N. Kutz, and S. L. Brunton. Deep learning for universal linear embeddings of nonlinear dynamics. *Nature Communications*, 9(1):4950, 2018.
- [39] A. J. Majda and J. Harlim. Physics constrained nonlinear regression models for time series. *Nonlinearity*, 26(1):201, 2012.
- [40] A. J. Majda and Y. Lee. Conceptual dynamical models for turbulence. *Proceedings of the National Academy of Sciences*, 111(18):6548–6553, 2014.
- [41] N. M. Mangan, S. L. Brunton, J. L. Proctor, and J. N. Kutz. Inferring biological networks by sparse identification of nonlinear dynamics. *IEEE Transactions on Molecular, Biological, and Multi-Scale Communications*, 2(1):52–63, 2016.
- [42] A. Mardt, L. Pasquali, H. Wu, and F. Noé. VAMPnets: Deep learning of molecular kinetics. *Nature Communications*, 9(5), 2018.
- [43] J. E. Marsden and T. S. Ratiu. *Introduction to mechanics and symmetry*. Springer-Verlag, 2nd edition, 1999.
- [44] I. Mezić. Spectral properties of dynamical systems, model reduction and decompositions. *Nonlinear Dynamics*, 41(1-3):309–325, 2005.
- [45] I. Mezić. Analysis of fluid flows via spectral properties of the Koopman operator. *Ann. Rev. Fluid Mech.*, 45:357–378, 2013.
- [46] I. Mezić. *Spectral operator methods in dynamical systems: Theory and applications*. Springer, 2017.
- [47] I. Mezić and A. Banaszuk. Comparison of systems with complex behavior. *Physica D: Nonlinear Phenomena*, 197(1):101–133, 2004.
- [48] I. Mezić and S. Wiggins. A method for visualization of invariant sets of dynamical systems based on the ergodic partition. *Chaos: An Interdisciplinary Journal of Nonlinear Science*, 9(1):213–218, 1999.
- [49] C. C. Moore. Ergodic theorem, ergodic theory, and statistical mechanics. *Proceedings of the National Academy of Sciences*, 112(7):1907–1911, 2015.

- [50] J. v. Neumann. Proof of the quasi-ergodic hypothesis. *Proceedings of the National Academy of Sciences*, 18(1):70–82, 1932.
- [51] F. Noé and F. Nuske. A variational approach to modeling slow processes in stochastic dynamical systems. *Multiscale Modeling & Simulation*, 11(2):635–655, 2013.
- [52] E. Noether. Invariante variationsprobleme nachr. d. könig. gesellsch. d. wiss. zu göttingen, math-phys. klasse 1918: 235-257. *English Reprint: physics/0503066*, [http://dx. doi. org/10.1080/00411457108231446](http://dx.doi.org/10.1080/00411457108231446), page 57, 1918.
- [53] F. Nüske, B. G. Keller, G. Pérez-Hernández, A. S. Mey, and F. Noé. Variational approach to molecular kinetics. *Journal of chemical theory and computation*, 10(4):1739–1752, 2014.
- [54] F. Nüske, R. Schneider, F. Vitalini, and F. Noé. Variational tensor approach for approximating the rare-event kinetics of macromolecular systems. *J. Chem. Phys.*, 144(5):054105, 2016.
- [55] S. E. Otto and C. W. Rowley. Linearly-recurrent autoencoder networks for learning dynamics. *arXiv preprint arXiv:1712.01378*, 2017.
- [56] S. Peitz and S. Klus. Koopman operator-based model reduction for switched-system control of PDEs. *arXiv preprint arXiv:1710.06759*, 2017.
- [57] L. Perko. *Differential equations and dynamical systems*, volume 7. Springer Science & Business Media, 2013.
- [58] J. L. Proctor, S. L. Brunton, and J. N. Kutz. Dynamic mode decomposition with control. *SIAM Journal on Applied Dynamical Systems*, 15(1):142–161, 2016.
- [59] J. L. Proctor and P. A. Eckhoff. Discovering dynamic patterns from infectious disease data using dynamic mode decomposition. *International health*, 7(2):139–145, 2015.
- [60] Q. Qu, J. Sun, and J. Wright. Finding a sparse vector in a subspace: Linear sparsity using alternating directions. In *Advances in Neural Information Processing Systems 27*, pages 3401—3409, 2014.
- [61] C. W. Rowley, I. Mezić, S. Bagheri, P. Schlatter, and D. Henningson. Spectral analysis of nonlinear flows. *J. Fluid Mech.*, 645:115–127, 2009.
- [62] T. P. Sapsis and A. J. Majda. Statistically accurate low-order models for uncertainty quantification in turbulent dynamical systems. *Proceedings of the National Academy of Sciences*, 110(34):13705–13710, 2013.
- [63] P. J. Schmid. Dynamic mode decomposition for numerical and experimental data. *J. Fluid. Mech*, 656:5–28, 2010.
- [64] P. J. Schmid and J. Sesterhenn. Dynamic mode decomposition of numerical and experimental data. In *61st Annual Meeting of the APS Division of Fluid Dynamics*. American Physical Society, Nov. 2008.
- [65] A. S. Sharma, I. Mezić, and B. J. McKeon. Correspondence between Koopman mode decomposition, resolvent mode decomposition, and invariant solutions of the Navier-Stokes equations. *Physical Review Fluids*, 1(3):032402, 2016.
- [66] W.-H. Steeb and F. Wilhelm. Non-linear autonomous systems of differential equations and Carleman linearization procedure. *Journal of Mathematical Analysis and Applications*, 77(2):601–611, 1980.
- [67] A. Surana. Koopman operator based observer synthesis for control-affine nonlinear systems. In *55th IEEE Conference on Decision and Control (CDC)*, pages 6492–6499, 2016.
- [68] A. Surana and A. Banaszuk. Linear observer synthesis for nonlinear systems using Koopman operator framework. *IFAC-PapersOnLine*, 49(18):716–723, 2016.
- [69] Y. Susuki and I. Mezić. A prony approximation of Koopman mode decomposition. In *Decision and Control (CDC), 2015 IEEE 54th Annual Conference on*, pages 7022–7027. IEEE, 2015.
- [70] A. Svenkeson, B. Glaz, S. Stanton, and B. J. West. Spectral decomposition of nonlinear systems with memory. *Phys. Rev. E*, 93:022211, Feb 2016.
- [71] S. Svoronou, D. Papageorgiou, and C. Tsiligiannis. Discretization of nonlinear control systems via the Carleman linearization. *Chemical engineering science*, 49(19):3263–3267, 1994.
- [72] N. Takeishi, Y. Kawahara, and T. Yairi. Learning Koopman invariant subspaces for dynamic mode decomposition. In *Advances in Neural Information Processing Systems*, pages 1130–1140, 2017.
- [73] F. Takens. Detecting strange attractors in turbulence. *Lecture Notes in Mathematics*, 898:366–381, 1981.
- [74] J. H. Tu, C. W. Rowley, D. M. Luchtenburg, S. L. Brunton, and J. N. Kutz. On dynamic mode decom-

- position: theory and applications. *J. Comp. Dyn.*, 1(2):391–421, 2014.
- [75] C. Wehmeyer and F. Noé. Time-lagged autoencoders: Deep learning of slow collective variables for molecular kinetics. *The Journal of Chemical Physics*, 148(241703), 2018.
- [76] M. O. Williams, I. G. Kevrekidis, and C. W. Rowley. A data-driven approximation of the Koopman operator: extending dynamic mode decomposition. *Journal of Nonlinear Science*, 6:1307–1346, 2015.
- [77] M. O. Williams, C. W. Rowley, and I. G. Kevrekidis. A kernel approach to data-driven Koopman spectral analysis. *Journal of Computational Dynamics*, 2(2):247–265, 2015.
- [78] E. Yeung, S. Kundu, and N. Hodas. Learning deep neural network representations for Koopman operators of nonlinear dynamical systems. *arXiv preprint arXiv:1708.06850*, 2017.